Radical generation and fate control for photocatalytic biomass conversion

Zhipeng Huang[1,2], *Nengchao Luo*[1], *Chaofeng Zhang*[1] *and Feng Wang*[1] ✉

Abstract | Photocatalysis is an emerging approach for sustainable chemical production from renewable biomass under mild conditions. Active radicals are always generated as key intermediates, in which their high reactivity renders them versatile for various upgrading processes. However, controlling their reaction is a challenge, especially in highly functionalized biomass frameworks. In this Review, we summarize recent advanced photocatalytic systems for selective biomass valorization, with an emphasis on their distinct radical-mediated reaction patterns. The strategies for generating a specific radical intermediate and controlling its subsequent conversion towards desired chemicals are also highlighted, aiming to provide guidance for future studies. We believe that taking full advantage of the unique reactivity of radical intermediates would provide great opportunities to develop more efficient photocatalytic systems for biomass valorization.

Photo-generated carriers
Electronic carriers (including negatively charged electrons and positively charged holes) generated from light-excited semiconductors. When a photon with energy larger than the bandgap energy is absorbed by the semiconductor, an electron is excited into the conduction band, while creating a hole in the valence band.

[1]*State Key Laboratory of Catalysis, Dalian National Laboratory for Clean Energy, Dalian Institute of Chemical Physics, Chinese Academy of Sciences, Dalian, China.*

[2]*University of Chinese Academy of Sciences, Beijing, China.*

✉*e-mail: wangfeng@dicp.ac.cn*

https://doi.org/10.1038/s41570-022-00359-9

Biomass is the largest renewable carbon resource in the world, with more than 170 billion tonnes of biomass produced annually from photosynthesis in nature. Thereby, the exploitation of biomass offers great potential for sustainable chemical supply, as an alternative to current fossil-fuel-based chemical manufacturing industries[1,2]. A shift to renewable carbon resources would directly reduce our dependence on fossil fuels and alleviate concerns about excessive CO_2 emissions and the resulting climate change[3]. To transform biomass components into desirable products, efficient strategies and protocols are required to selectively cleave biomass polymer crosslinks or controllably upgrade platform molecules that can be readily attained from raw biomass (FIG. 1). For instance, lignin, one of the major components of lignocellulose, is a complex polymer consisting of various methoxylated phenylpropanoid units[4]; selective scission of the crosslinked C–C/C–O bonds would release value-added aromatic products, such as benzaldehydes and phenols. Moreover, deoxygenation of lipid-derived fatty acids could deliver long-chain alkanes that can be directly used as diesel and jet fuel.

Photocatalysis that can harness light energy — especially inexhaustible solar energy, to drive the redox reactions — has been recognized as an emerging approach for biomass conversion[5–7] (BOX 1). A photocatalytic process typically initiates with electron transfer between the excited photocatalyst and the biomass substrate, which facilely generates active radical species as key intermediates. Owing to their special electronic structures (unpaired electrons) and energetic nature, these radical intermediates can readily undergo various downstream conversions — including some energetically or kinetically difficult transformations — under mild conditions[7,8]. For instance, the formation of a specific oxygen or carbon radical in lignin linkages by the photocatalytic approach can dramatically weaken the adjacent chemical bonds, or even directly lead to a spontaneous bond scission reaction at room temperature, whereas thermocatalytic bond scission reactions generally necessitate relatively high temperatures (>150 °C) and stoichiometric reductant/oxidant[4,9].

Despite the versatility of radical intermediates for various upgrading processes, the active reactivity when induced by light brings great challenges to control the following reactions, especially for the conversion of highly functionalized biomass feedstock[10]. On stimulation of light-induced active species (for example, photo-generated carriers on semiconductor photocatalyst), multiple sites in the biomass component are simultaneously activated to furnish diverse radicals, in which each radical species has its own reaction pathway. Therefore, the downstream conversion of undesired radical intermediates competes with the targeted process. For example, furfural, a typical platform compound derived from carbohydrates, can be reduced into the corresponding ketyl or alkoxy radical over excited TiO_2 catalysts, leading to distinct product distribution[11]. Hence, a complex mixture would be attained without proper control. Furthermore, the subsequent conversion of active radical intermediates is very fast and sensitive to their local chemical environment, which includes the adjacent functional groups and structures, reaction conditions and catalysts[12–14]. Therefore, a delicate design is

Key points

- Photocatalysis is an efficient approach for value-added chemical production from renewable biomass under mild conditions.
- The active and energetic nature of light-induced radical intermediates offers unique reaction patterns for selective biomass valorization, but efficient strategies for manipulating their generation and subsequent conversion are needed.
- The formation of a specific radical intermediate from biomass substrates is the prerequisite for selective biomass upgrading by photocatalysis, which relies greatly on the rational design of catalytic systems.
- The introduction of suitable extraneous radical species is an alternative solution to achieve challenging transformations.
- Subtly tuning the interactions between catalyst and light-induced radical species is imperative to modulate the conversion of radical intermediates towards desired products.

needed for the catalytic system to regulate the conversion of radicals, that is, to make sure that the conversion pathway that leads to the final valuable product is the most energetically and/or dynamically favourable one. Otherwise, an unregulated radical network would lead to a low reaction efficiency. Consequently, controlling the reactions of radical intermediates is imperative for selective chemical production from biomass conversion, and comprehensive understandings of the radical chemistry in photocatalysis are essential for the design of valid strategies and protocols.

This Review summarizes recent advanced photocatalytic systems for value-added chemical production from various raw biomass and derivatives, with specific attention on their efficient strategies with active radical intermediates (FIG. 1). Two basic aspects are introduced in detail. The formation of a specific radical intermediate from biomass component activation is first described, as it is the prerequisite for selective biomass valorization by photocatalysis. Then, we concentrate on the interactions between the generated radical intermediate and the catalyst, and their effect on modulating the subsequent conversion of radical species towards desired reactions. Radical control in photocatalytic biomass conversion is vital for the further development of such a promising process.

Generating specific radicals

As radical species with unpaired electrons are known for their high reactivity[12], activation of biomass components to a specific radical intermediate that undergoes an upgrading process, such as bond scission or C–C bond coupling reaction, is essential for selective biomass valorization. For instance, for lignin conversion, the key issue is to break down interunit linkages to release valuable aromatic monomers. Thereby, generating a radical intermediate that lowers the bond dissociation enthalpy (BDE) of targeted C–C/C–O bonds or provides new active sites for the introduction of cleavage reagent would significantly promote the subsequent bond scission reaction[9]. In this section, we exemplify recent effective photocatalytic protocols for chemical production from biomass by forming specific radical intermediates. The corresponding reaction patterns and especially their valid strategies for accessing key radical species are discussed in detail; the biomass feedstocks include lignin linkages and carbohydrate-derived furfurals.

Back electron transfer
Refers to the deactivation/quenching process of the activated substrate by charged species. After stimulation by a positively charged hole, for example, the activated substrate reacts with electron or hydrogen species and subsequently reforms to its initial state.

Oxygen-radical-induced lignin C–C bond cleavage. The formation of alkoxy radical from O–H bond activation could remarkably weaken the adjacent C–C bond, thus, enabling the β-scission, which is a valid protocol to realize the ring-opening reaction of various cyclic alcohols[15,16]. Given the ubiquitous existence of hydroxyl groups in lignin, such as the lignin *β*-O-4 and *β*-1 linkages, the C–C bond rupture method is expected to be an effective protocol to fragment the lignin structure for value-added aromatic production. However, the C_α–H bond always competes with the desired O–H bond to be activated due to its relatively lower oxidation potential. Taking the lignin *β*-O-4 model as an example, the oxidation potential for the benzyl C_α–H bond is about 0.4 V lower than that of the O–H bond[17]. Therefore, the preferential formation of alkoxy radical in lignin linkage necessitates the development of novel catalytic strategies (FIG. 2a).

Owing to the relatively strong polarity, the O–H bond can be easily activated in the presence of a base (pathway B in FIG. 2a). A proton-coupled electron transfer (PCET) process was developed to activate the O–H bond, followed by β-scission to cleave the C–C bond in both *β*-O-4 and *β*-1 linkages at room temperature under photoredox-neutral condition[18] (FIG. 2b). Choosing a suitable base is vital for the PCET process to furnish the key alkoxy radical, and collidine is the optimal one in this case. The reaction initiates with the electron transfer between excited photocatalyst $^*Ir^{III}$ and the phenyl moiety of the substrate, delivering a radical cation intermediate (FIG. 2c). Then, the radical cation is transformed into the key alkoxy radical through a PCET process with the aid of collidine, which subsequently undergoes β-scission to produce benzaldehyde and another carbon radical. Finally, the hydrogen atom donor, thiophenol, quenches the generated carbon radical and oxidizes the reduced Ir photocatalyst, thereby, enclosing the catalytic cycle. Under blue light-emitting diodes (LEDs; 50 W) irradiation, both lignin *β*-O-4 and *β*-1 models can be converted into corresponding products with high yields (>90%) after 12 h of reaction. However, this method is inefficient for the direct fragmentation of birch dioxane lignin due to the presence of numerous phenolic structures in lignin. The phenolic hydroxyl group is an excellent moiety for the PCET process, which significantly completes with the α-OH group to be activated[19]. Meanwhile, the generated phenoxy radical could not undergo productive chemistry, and, instead, it would reform to the initial substrate via a back electron transfer process[20]. Therefore, the unwanted activation of the phenolic hydroxyl group would significantly slow down, or even completely block, the targeted C–C bond scission reaction. Only after a pretreatment with iodomethane and K_2CO_3 to protect the hydroxyl groups on the phenoxy rings can the birch dioxane lignin be converted by this method to offer degraded products with a yield of 4.99 wt% after blue LEDs (100 W) irradiation for 12 h. In a latter study, based on the large differential of bond strength between the phenolic and aliphatic O–H bonds, an optimized PCET system was developed that is compatible with the phenolic hydroxyl group in lignin substrates[20]. Various native lignin can be directly depolymerized without any pretreatment under blue

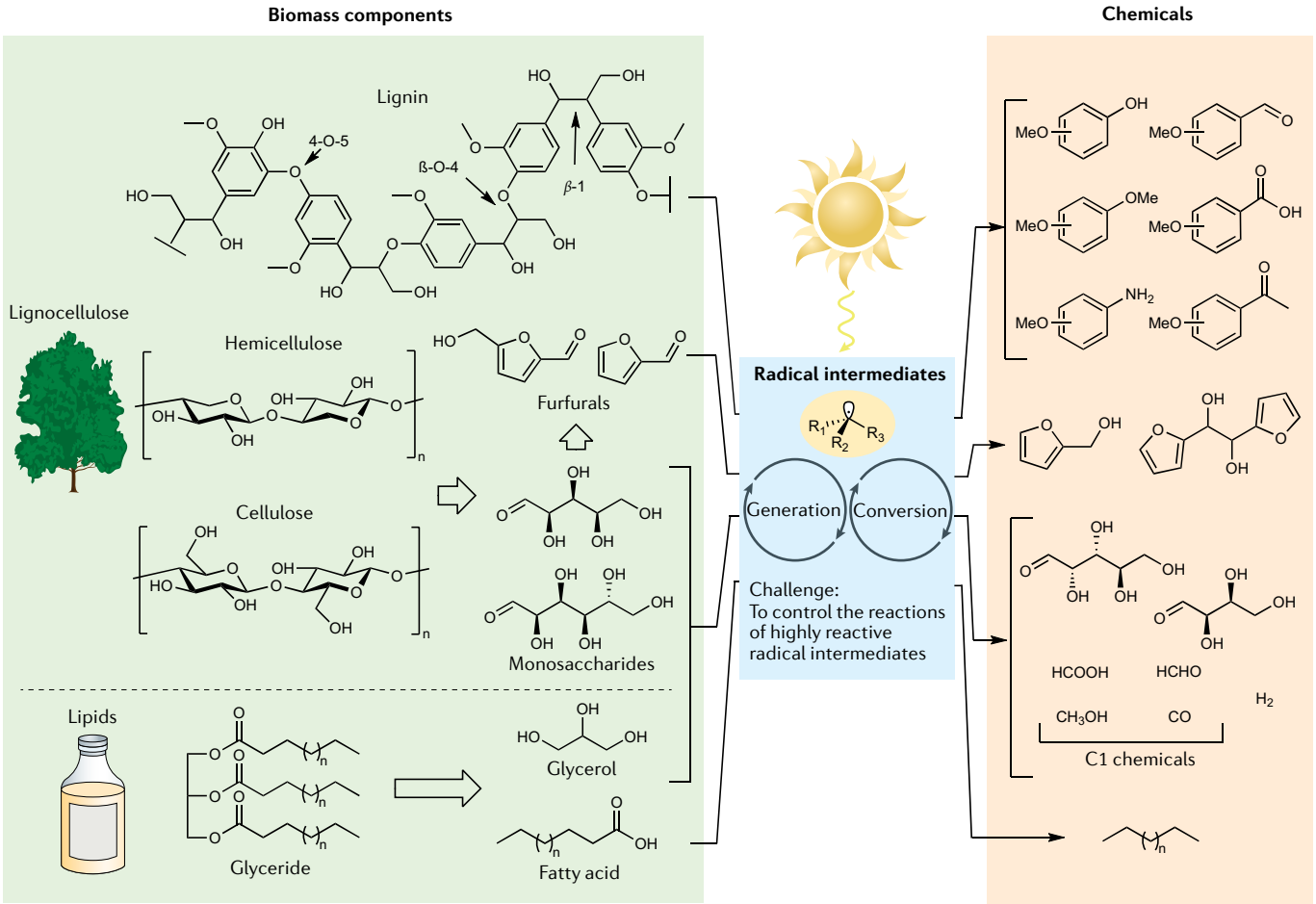

Fig. 1 | **Schematic representation of chemical production from renewable biomass via radical-mediated photocatalytic pathways.** All the conversion processes involved in this Review are shown. Subtly controlling the reactions of radical intermediates is pivotal to the reaction efficiency of photocatalytic biomass conversion.

LEDs irradiation, offering monomer products with yields from 3.4 to 5.1 wt% at a reaction time of 48 h. In addition to the Ir-based catalysts, an acridinium salt/copper catalytic system was developed to break down the C_α–C_β bond in lignin β-O-4 and β-1 models via a similar alkoxy-radical-mediated mechanism[21]. Under irradiation, the excited acridinium photocatalyst transforms the lignin model into an alkoxy radical with the aid of NaOAc that works as a base. The resulting alkoxy radical then undergoes β-scission to produce benzaldehyde and a carbon radical, which was further converted into phenyl formate or another molecule of aldehyde under aerobic conditions in the presence of a copper catalyst.

The chelation ability of the benzyl α-OH group offers another route for the preferential formation of alkoxy radicals on light excitation. If a catalytically active metal coordinates with the α-OH group of lignin substrates, a light-induced ligand-to-metal charge transfer (LMCT) process would also lead to the generation of alkoxy radical and subsequent C_α–C_β bond scission (pathway C in FIG. 2a). A novel vanadium complex was developed that can cleave the C_α–C_β bond in lignin β-O-4 linkage via such a LMCT mechanism under aerobic conditions[22]. Under irradiation, the lignin model compound can be degraded into the corresponding benzaldehyde and phenyl formate in moderate yields. Following this development, a class of molecular V^V oxo complexes was synthesized by rational ligand modification[23]. The catalysts with stronger oxidative ability were more favourable for the targeted C–C bond cleavage. As such, these new candidates are up to seven times faster than their original vanadium complex for lignin model conversion. This LMCT strategy is applicable to the cleavage of C_α–C_β bonds in both lignin β-O-4 and β-1 linkages[24]. Much simpler vanadium-based photocatalysts were used in this case. Under blue LEDs (6 W) irradiation, the lignin β-1 model can be converted into two molecules of benzaldehyde in 86% yield over $VO(O^iPr)_3$ catalyst, while $VO(acac)_2$ with a small amount of N-hydroxyphthalimide is the optimal candidate for the conversion of the lignin β-O-4 model. This method can be used for the depolymerization of various dioxasolv lignin, but the monomer yields are unsatisfying (<1.5 wt% after 24 h of reaction). Both the distinct oxidative ability of V^V catalysts and the chelating interaction with the targeted hydroxyl group are crucial for these C–C bond scission processes.

Recently, a cerium(III) chloride ($CeCl_3$)-promoted photocatalytic bond scission strategy was reported for

Box 1 | **Fundamentals of photocatalytic biomass conversion**

Semiconductors and molecular photocatalysts (MPCs) are the most frequently applied catalysts for photocatalytic biomass conversion; their corresponding mechanisms are briefly introduced herein. In semiconductor photocatalysis, when a photon with energy larger than the bandgap energy is absorbed by the semiconductor, an electron is excited into the conduction band, while creating a hole in the valence band (see the figure, panel **a**). Then, the separated electron–hole pair can migrate to the surface to interact with the biomass substrates and initiate the reaction. MPCs mainly include transition metal complexes and organic photocatalysts, such as acridinium salts and phenothiazine. Under irradiation, the MPC is stimulated into its excited state, which directly induces the electron transfer with the biomass substrates (see the figure, panel **b**). The biomass feedstock can act as an electron acceptor or donor, depending on its intrinsic structure and the photocatalyst used.

Radical species are generally formed as key intermediates as a result of the electron transfer between excited photocatalysts and biomass substrates. Owing to their active and energetic nature, they could facilely undergo the downstream transformations with a very low or even zero energy barrier (routes II and III in panel **c**, respectively). However, efforts to subtly control the radical-involved reactions are imperative to improve the efficiency of photocatalytic biomass conversion.

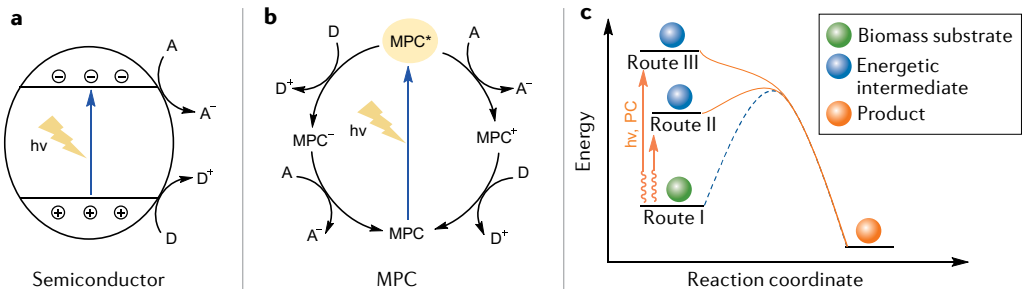

A, electron acceptor; D, electron donor.

lignin depolymerization with simultaneous production of an N-containing chemical[25] (FIG. 3). Taking the conversion of the lignin β-O-4 model as an example, this process initiates with the formation of a $Ce^{III}Cl_n$/lignin complex through the deprotonation of the α-OH group, which is successively oxidized by di-*tert*-butyl azodicarboxylate to generate a $Ce^{IV}Cl_n$/lignin species. Subsequently, a light-induced homolysis of the high-valent species via the LMCT mechanism delivers the key alkoxy radical followed by β-scission to produce benzaldehyde and a carbon radical intermediate. In previous cases, this radical is quenched by a hydrogen atom donor or react with oxygen species to produce corresponding ether and formate, respectively[18,24]. However, the carbon radical here is coupled with di-*tert*-butyl azodicarboxylate to furnish substituted hydrazinium compounds. Under optimized conditions, various lignin β-O-4 model compounds can be converted into benzaldehyde and hydrazinium in yields up to 96% and 95%, respectively (FIG. 3b). Moreover, this system can be used for the depolymerization of natural pine lignin, and an impressive yield of monomers (11.94 wt%) was attained (FIG. 3c).

Carbon-radical-mediated oxidative lignin C–C bond cleavage. In addition to the initial generation of an alkoxy radical, selective activation of the C_β–H bond would also provide an oxidative method for the cleavage of C_α–C_β bonds in both lignin β-O-4 and β-1 linkages. Taking the conversion of the lignin β-1 model as an example[26] (FIG. 4a), the first activation of the C_α–H bond leads to the oxidation of the C_αH–OH moiety to the C_α=O group, which increases the BDE of the C_α–C_β bond from 70.4 to 84.6 kcal mol^{-1}. Therefore, the targeted bond cleavage would be dramatically inhibited. On the other hand, the C_β radical derived from C_β–H bond activation can combine with a superoxide anion derived from electron-mediated O_2 reduction, delivering an active peroxide intermediate. The latter will undergo dehydration and C_α–C_β bond cleavage to form benzaldehyde through a six-membered-ring transition state. Consequently, the key to desired C_α–C_β bond cleavage in β-1 linkage lies in the preferential activation of the C_β–H bond.

In 2017, a hybrid CuO_x/ceria/TiO_2 (anatase) catalyst was synthesized that can promote the C–C bond scission in lignin β-1 linkage with high selectivity under visible light irradiation[26]. The fabrication of highly dispersed CuO_x nanoclusters on a catalyst surface is pivotal for the selective C_β–H bond activation. CeO_2/TiO_2 can catalyse the C–C bond cleavage of the lignin β-1 model (1,2-diphenylethanol) with a moderate selectivity (75%); the ketone counterpart derived from the oxy-dehydrogenation of the hydroxyl group was generated as the major by-product (FIG. 4b). The control experiment revealed that the C_α–H bond activation mainly occurred on TiO_2. In order to suppress the side reaction, CuO_x nanoclusters were decorated on the catalyst surface. The density of states calculation proved that the valence band maximum (VBM) of CuO_x/TiO_2 is primarily constituted by Cu3d orbit, indicating that photo-generated holes would transfer to CuO_x nanoclusters predominantly. Meanwhile, CuO_x nanoclusters are inactive for C_α–H bond cleavage, so they can act as hole-trapping centres and block the unwanted side reactions on TiO_2 (FIG. 4c,d). Moreover, the CuO_x nanoclusters in intimate contact with ceria further improve the concentration of oxygen vacancy (V_O) on ceria, the catalytically active site of ceria[27]. Consequently, compared with the ceria/TiO_2 catalyst, the CuO_x/ceria/TiO_2 hybrid

Density of states
A physical concept to describe the proportion of states that are to be occupied by the system at each energy level.

Photo-generated holes
Positively charged species generated from light-excited semiconductors.

Hole-trapping centres
Refers to the catalyst sites that can trap free photo-generated holes.

catalyst is significantly more efficient for C–C bond scission, and it can realize the complete conversion of the lignin β-1 model with a 99% selectivity of benzaldehyde. In a later study, a mesoporous graphitic carbon nitride (mpg-C_3N_4) catalyst could efficiently cleave the C_α–C_β bond in both lignin β-O-4 and β-1 linkages under visible light irradiation, which follows a similar mechanism with the formation of C_β radical as the initial step[28]. Experimental and theoretical studies indicate an intimate π–π stacking interaction between the flexible carbon nitride surface and the lignin model molecule, which may facilitate the preferential C_β–H bond activation by a photo-generated hole. These studies verify the importance of rational photocatalyst design for site-selective radical activation.

In 2019, a model was reported of a photochemical method for the oxidative cleavage of C_α–C_β bonds in pre-oxidized lignin β-O-4 by the sequential participation of two functional ionic liquids (ILs)[29] (FIG. 4e). This bond scission begins with C_β–H bond activation

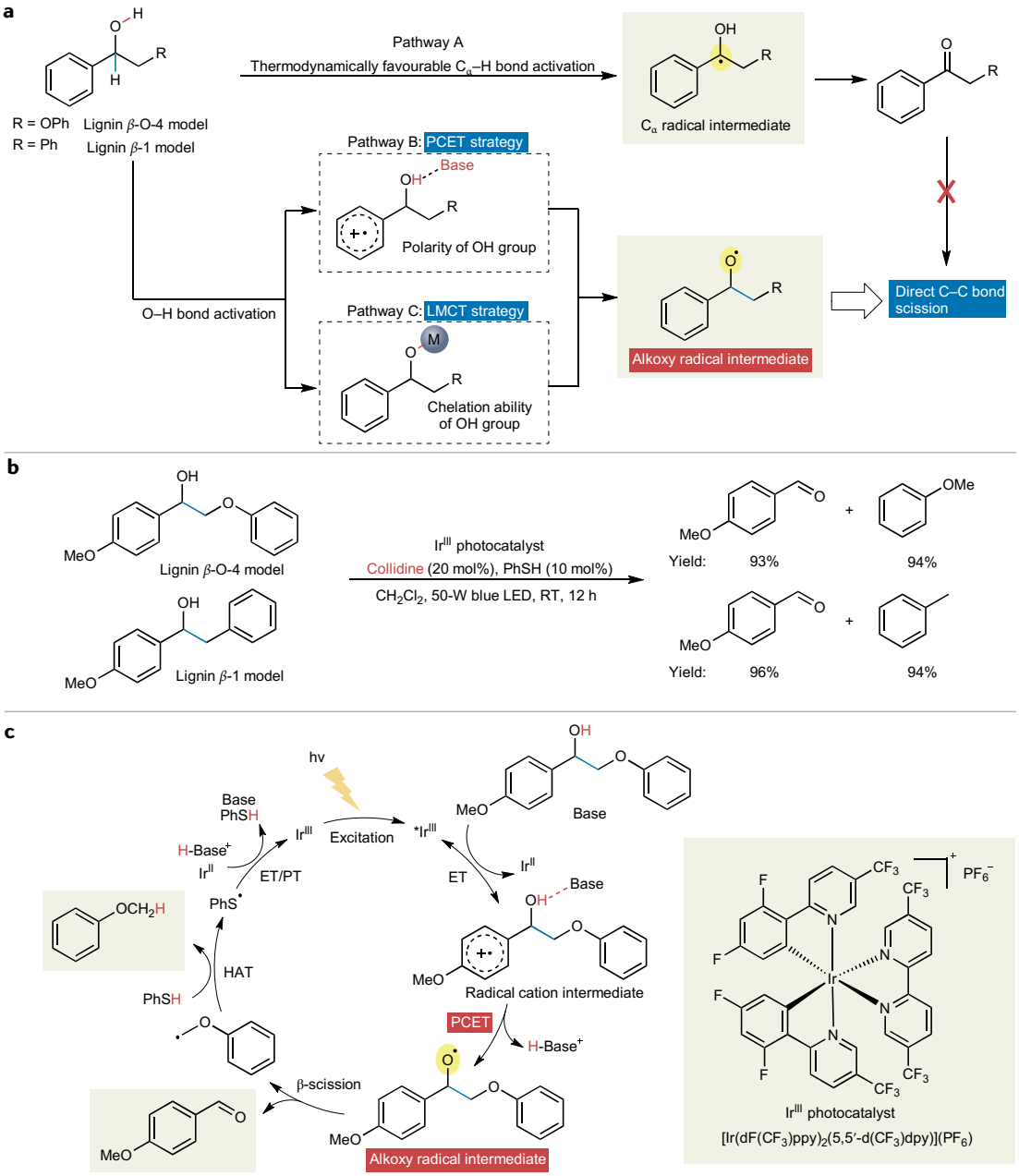

Fig. 2 | **Strategies for preferential activation of O–H bond and C_α–C_β bond cleavage in lignin β-O-4 and β-1 linkages.** **a** | Pathway A represents the C_α–H bond activation pathway on stimulation of photo-generated hole. Pathways B and C show the strategies of selective O–H bond activation via proton-coupled electron transfer (PCET) or ligand-to-metal charge transfer (LMCT), respectively. **b** | Photocatalytic C_α–C_β bond cleavage of lignin β-O-4 and β-1 linkages via the PCET process[18]. **c** | Proposed mechanism for lignin bond cleavage via PCET process. The bond cleavage is proposed to be mediated by an alkoxy radical derived from the PCET process[18]. ET, electron transfer; HAT, hydrogen atom abstraction; LED, light-emitting diode; PT, proton transfer; RT, room temperature. Panel **c** adapted with permission from REF.[18], Elsevier.

to deliver a C_β radical with the aid of [Pmin][NTf_2] IL (1-propenyl-3-methylimidazolium bis[(trifluoromethyl)sulfonyl] imide) under ultraviolet (UV) light irradiation. The strong electronegativity of this IL is vital to this initiation step. Subsequently, the C_β radical reacts with atmospheric oxygen to form the peroxy radical, which further abstracts proton from water to form a hydroperoxide intermediate and a hydroxyl radical. The hydroperoxide is eventually transformed into benzoic acid and phenol via C–C bond scission catalysed by an acidic IL, [$PrSO_3HMim$][OTf] (1-propylsulfonic-3-methylimidazolium trifluoromethanesulfonate). Thereby, the formation of peroxide species from C_β–H bond activation is a pathway for the fragmentation of both lignin β-O-4 and β-1 linkages, as similar mechanisms were also proposed in other thermocatalytic and electrocatalytic systems[30–32]. It should be noted that this method generally involves the participation of active oxygen species (for example, peroxy and hydroxyl radicals), which makes it less compatible with the labile phenolic moiety, thus, limiting its application in the fragmentation of native lignin.

Cation-radical-mediated lignin bond cleavage. In spite of the structural rigidity of lignin, some enzymes from wood-rotting fungi, such as lignin peroxidase, are efficient for lignin depolymerization through cation-radical-mediated C–C bond cleavage pathways[33]. In order to gain comprehensive insight into this unique bond cleavage process and mimic the enzymatic reactions, fragmentation of various lignin model compounds were investigated by using 9,10-dicyanoanthracene (DCA) as an electron acceptor to initiate the reaction under light irradiation[34–36] (FIG. 5a). Owing to its strong oxidative ability ($E^{DCA*/DCA-\bullet}$ = +2.8 V versus saturated calomel electrode (SCE)), the excited DCA can readily oxidize the dimeric lignin β-O-4 and β-1 models into corresponding aryl cation radicals through a single-electron transfer (SET) process, resulting in a dramatic decrease in the BDE of C_α–C_β bonds[34]. The interactions

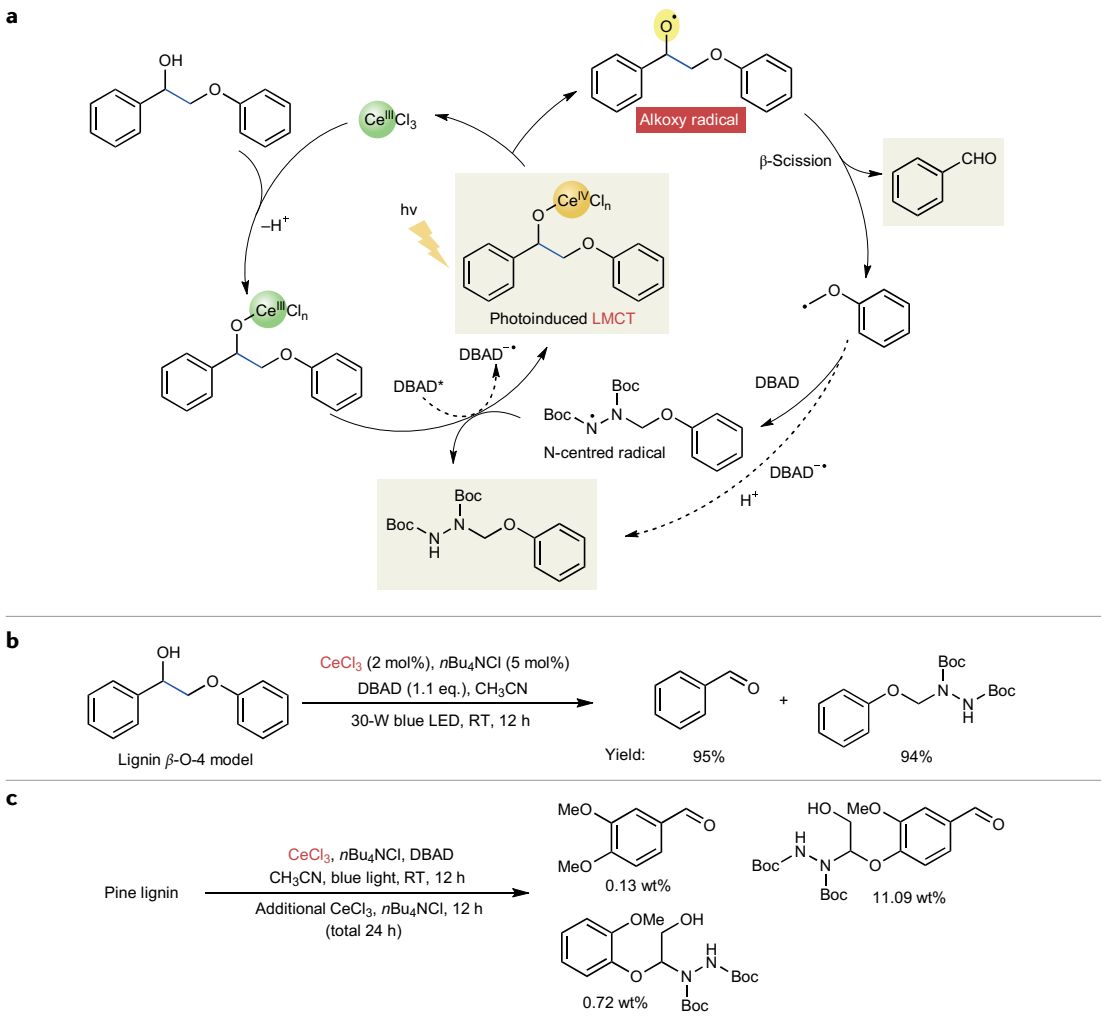

Fig. 3 | **$CeCl_3$-promoted photocatalytic C_α–C_β bond cleavage in lignin β-O-4 linkage via LMCT process. a** | Bond cleavage is triggered by a light-induced ligand-to-metal charge transfer (LMCT) process on a $Ce^{IV}Cl_n$/lignin species[25]. **b** | Optimized conditions for the pathway in part **a** to result in high yields[25]. **c** | Depolymerization of natural pine lignin[25]. DBAD, di-*tert*-butyl azodicarboxylate; LED, light-emitting diode; RT, room temperature. This figure has been published in *CCS Chemistry* 2020; $CeCl_3$-promoted simultaneous photocatalytic cleavage and amination of C_α–C_β bond in lignin model compounds and native lignin is available online at https://doi.org/10.31635/ccschem.020.201900076.

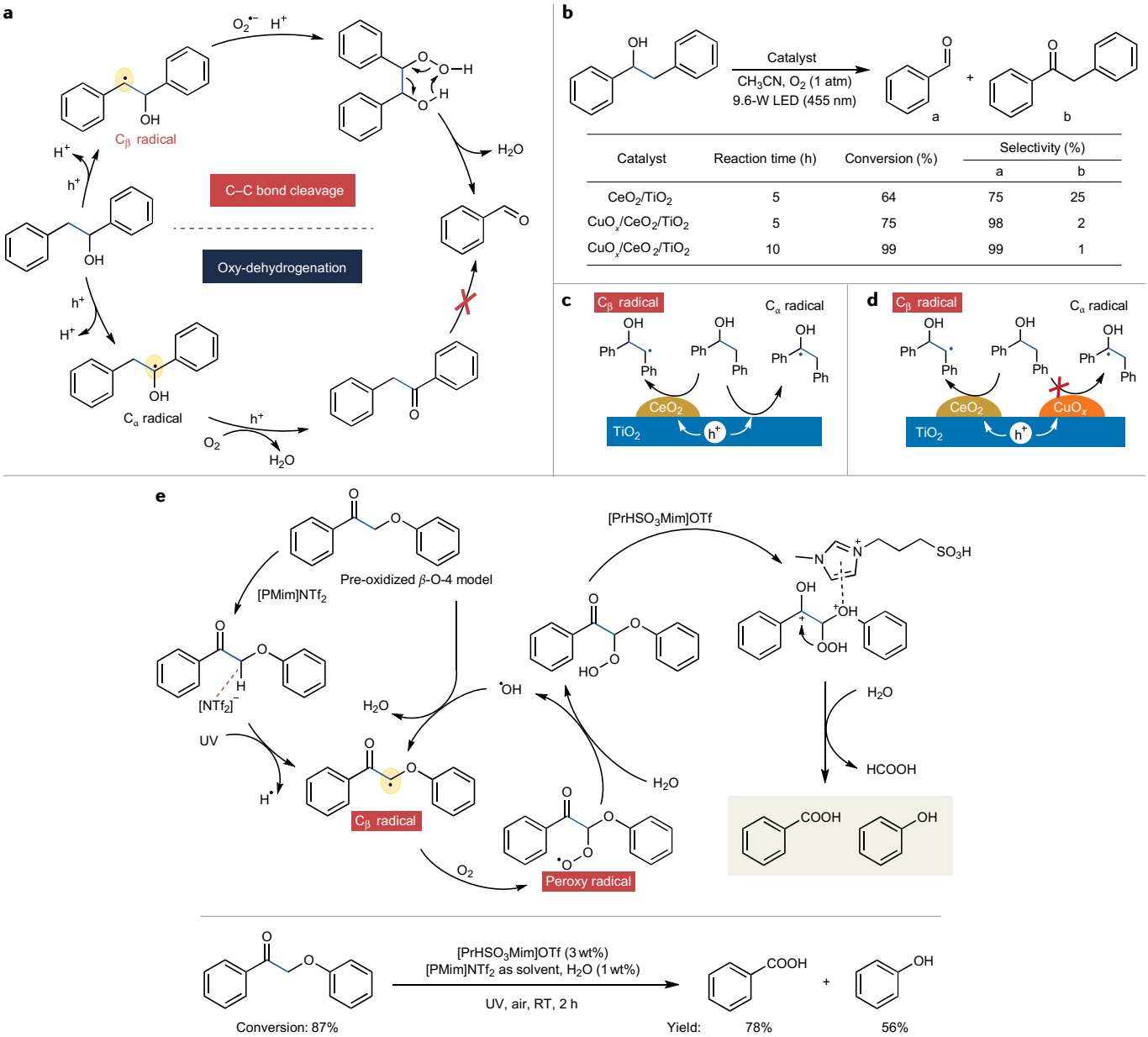

Catalyst	Reaction time (h)	Conversion (%)	Selectivity (%)	
			a	b
CeO_2/TiO_2	5	64	75	25
$CuO_x/CeO_2/TiO_2$	5	75	98	2
$CuO_x/CeO_2/TiO_2$	10	99	99	1

Fig. 4 | **Carbon-radical-mediated oxidative lignin C–C bond cleavage. a** | Photocatalytic oxidative C_α–C_β bond cleavage in lignin β-1 linkage over CuO_x/ceria/TiO_2. Proposed reaction pathways of lignin β-1 model conversion[26]. **b** | Photocatalytic lignin β-1 model conversion over different catalysts[26]. **c**,**d** | Schematic conversion of the lignin β-1 model over ceria/TiO_2 (panel **c**) and CuO_x/ceria/TiO_2 (REF.[26]) (panel **d**). **e** | Dual ionic liquid (IL)-promoted photochemical degradation of the pre-oxidized lignin β-O-4 model. The conversion is initiated by IL-assisted C_β–H bond activation under ultraviolet (UV) irradiation, and the bond cleavage is mediated by a hydroperoxide intermediate with the aid of an acidic IL[29]. LED, light-emitting diode; RT, room temperature. Panels **a**–**d** adapted with permission from REF.[26], American Chemical Society. Panel **e** adapted with permission from REF.[29], Wiley.

between the arene π-system and the weakened σ-bond would lead to C_α–C_β bond cleavage of the cation radical intermediates. It is notable that this C–C bond scission of β-1 models takes place more rapidly than that of the β-O-4 counterparts because of their lower C_α–C_β bond BDE of the corresponding cation radical intermediates. More interestingly, for the photoconversion of the tetrameric lignin model containing both β-O-4 and β-1 linkages, four benzene rings can be simultaneously activated into the corresponding cation radical centres by the excited DCA because of their very similar oxidation potentials, but the tetrameric substrate always preferentially undergoes the C–C bond cleavage in its β-1 subunit[35] (FIG. 5b). These results illustrate that the bond scission reactions of lignin cation radicals are governed by reactivity rather than electronic population. Despite the validity of this protocol for lignin fragmentation, some labile products, such as phenols, are always attained in low yields under highly oxidative conditions.

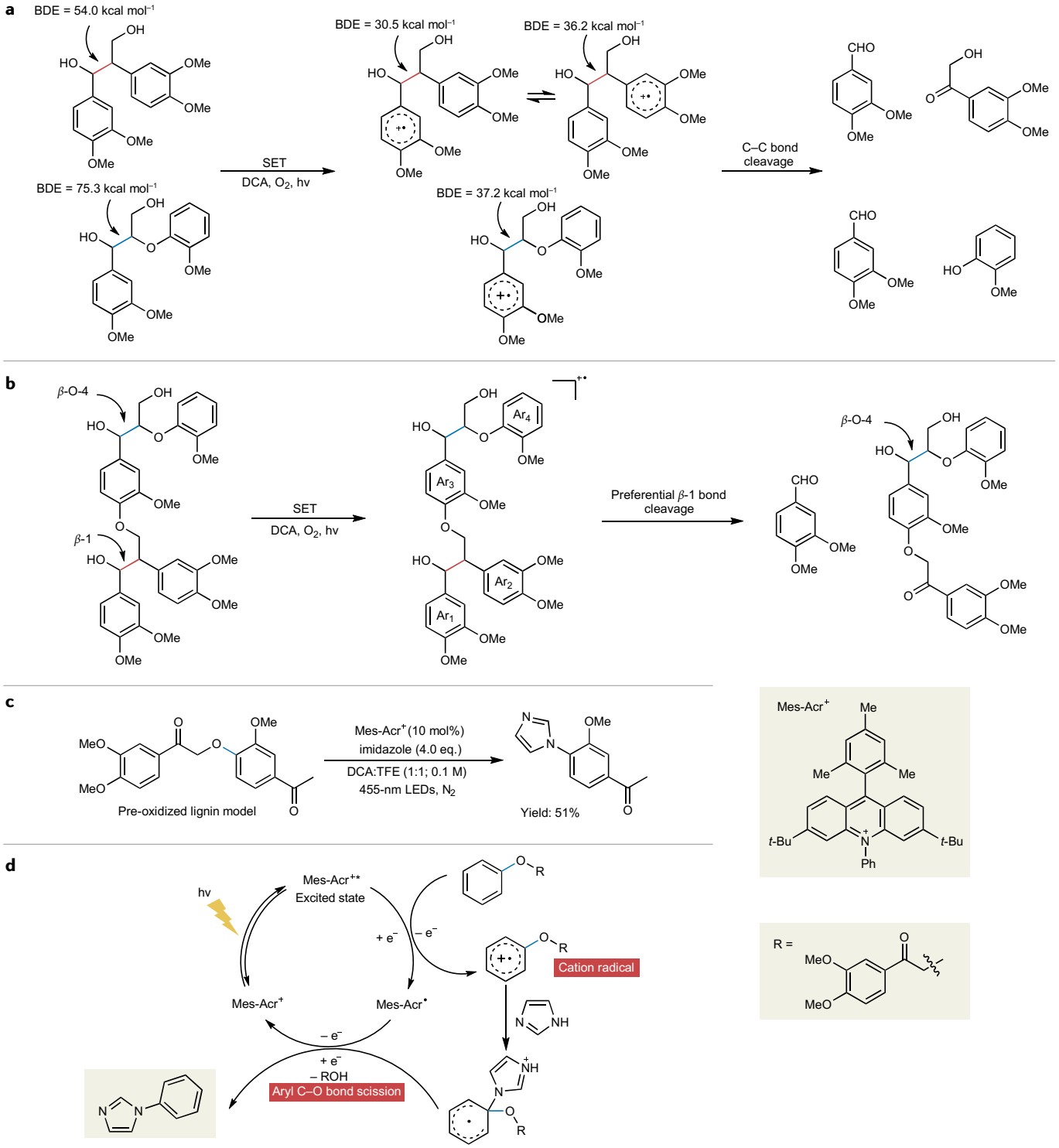

Fig. 5 | **Cation-radical-induced bond cleavage in dimeric, tetrameric and pre-oxidized lignin models. a**,**b** | C–C bond cleavage in dimeric[34] (panel **a**) and tetrameric[35] (panel **b**) lignin models triggered by excited 9,10-dicyanoanthracene (DCA). This method is more efficient for the cleavage of C–C bonds in β-1 (red) linkage compared with that in β-O-4 (blue) linkage. **c** | Cation-radical-mediated nucleophilic substitution for the cleavage of aryl C–O bonds in the pre-oxidized lignin model[37]. **d** | Proposed mechanism for the cation-radical-mediated nucleophilic substitution process. Imidazole species attack the electrophilic aryl cation radical to induce aryl C–O bond cleavage and form C–N bonds[37]. BDE, bond dissociation enthalpy; LED, light-emitting diode; Mes-Acr$^+$, 9-mesityl-10-methylacridinium ion; SET, single-electron transfer; TFE, 2,2,2-trifluoroethanol. Panels **c** and **d** adapted with permission from REF.[37], American Chemical Society.

Formation of the ketone counterpart from C_αH–OH moiety oxidation in lignin β-O-4 linkage restrains the cation-radical-mediated C–C bond cleavage reaction; however, it offers a new reaction pattern to use the cation radical intermediate as an active electrophile. In 2017, a novel nucleophilic aromatic substitution

strategy was developed to cleave the aryl C–O bond in the pre-oxidized lignin β-O-4 model to deliver valuable N-containing aromatics in moderate yield[37] (FIG. 5c,d). Upon irradiation, the electron-rich arene moiety is first oxidized into an open-shell cation radical by the photo-generated hole — the strong oxidative ability of excited acridinium photocatalyst (9-mesityl-10-methylacridinium ion ($Mes\text{-}Acr^+$)) ($E^{Mes\text{-}Acr^{+*}/Mes\text{-}Acr^{\bullet}} = +2.15$ V versus SCE) is pivotal to this reaction. Subsequently, nucleophilic attack on the *ispo*-position by imidazole species leads to ether bond cleavage under redox-neutral conditions. It is notable that this method can selectively cleave the aryl C–O bond while keeping the methoxyl groups on benzene rings intact.

Selective formation of oxygen/carbon radicals from furfural reduction. Carbohydrates can be readily transformed into a set of so-called platform molecules via commercialized technologies, which were initially defined by the US Department of Energy in 2004 (REFS[38,39]). Compared with the raw substrates, they are much less functionalized and relatively simple in chemical structure, which allows for better control over their subsequent transformation, and, thereby, higher selectivity towards targeted products. Furfurals are the most typical platform molecules derived from carbohydrate dehydration and have been intensively investigated for the production of valuable fuels and chemicals[40]. One approach is to use furfurals as building blocks to access C_9–C_{22} compounds, which can be blended into gasoline or directly used as diesel and jet fuels after hydrodeoxygenation[41]. Aldol condensation between furfurals and extra ketones is typically used to build up the carbon number in final products, which requires a base catalyst and relatively high temperatures (≥180 °C). Alternatively, activation by photo-generated carriers and subsequent radical coupling could provide an efficient pathway to furnish desired jet fuel precursors from furfurals under ambient conditions[42].

An investigation into the photoconversion of furfural in methanol over TiO_2 nanocrystals found an interesting morphology-dependent product distribution[11] (FIG. 6a). Furfural can be hydrogenated to furfural alcohol or undergo reductive coupling to produce hydrofuroin and furoin, initiated by a hydrogen transfer process from methanol. Both furfural alcohol and C–C coupling products can be obtained over bipyramid-shaped anatase (A-bipyramid) and anatase nanosheet (A-sheet) TiO_2 catalysts. Herein, the selectivity towards reductive coupling decreased with prolonged reaction time, which implies gradual evolution of surface structures on these two catalysts. By contrast, rod-shaped rutile TiO_2 (R-rod) catalyst can transform furfural into C–C coupling products with nearly 100% selectivity. Subsequent investigations with electron paramagnetic resonance and X-ray photoelectron spectroscopy revealed the existence of a substantial amount of V_O on both A-bipyramid and A-sheet and their progressive accumulation under UV irradiation in methanol, which accords with the trend of product distribution evolution during the reaction. On the other hand, a negligible amount of V_O was found on R-rod, and it changed marginally under irradiation. These results demonstrate the crucial role of V_O in

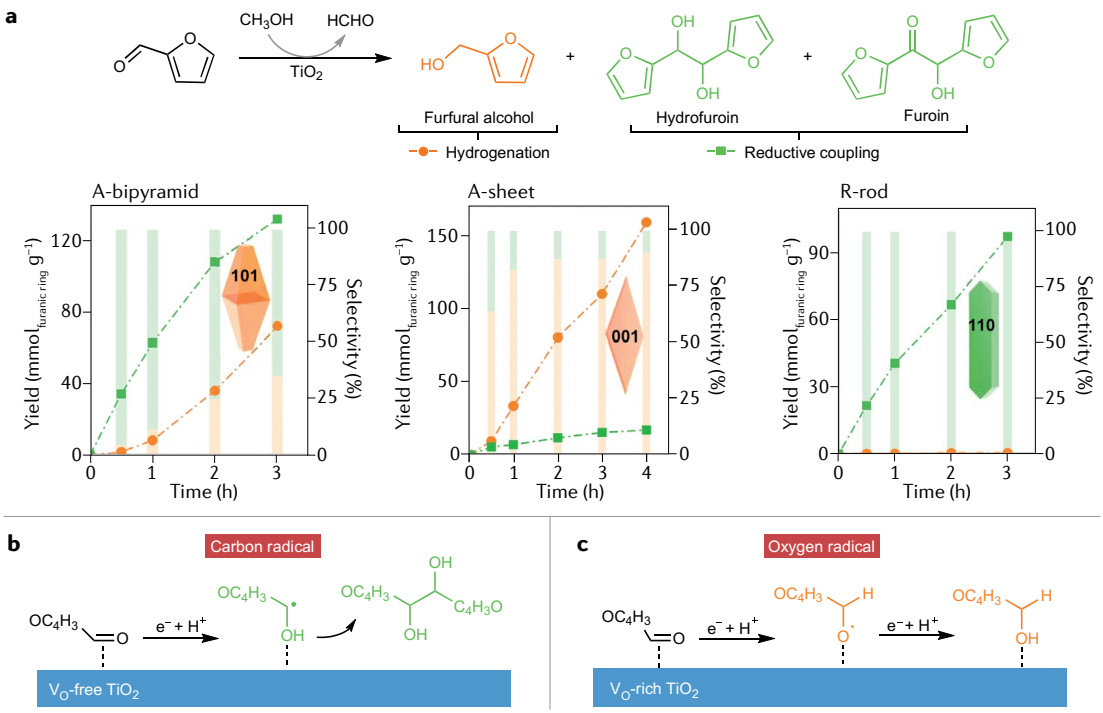

Fig. 6 | **Photocatalytic conversion of furfural over TiO_2.** Photocatalytic furfural conversion over different TiO_2 nanocrystals in methanol (panel **a**). The proposed mechanism for furfural conversion over V_O-free (panel **b**) and V_O-rich (panel **c**) TiO_2. A-bipyramid, bipyramid-shaped anatase; A-sheet, anatase nanosheet; R-rod, rod-shaped rutile TiO_2. Figure adapted with permission from REF.[11], Elsevier.

selective furfural conversion. On the V_O-free surface, the proton–electron pairs ($e^- + H^+$) are prone to attacking the negatively charged oxygen atoms of the carbonyl group to yield a carbon radical intermediate (•C–OH) (FIG. 6b). For example, on anatase (101) surface, this step is 0.54 eV more favourable than the first attack on the carbon atom of the carbonyl group according to density functional theory calculations. Moreover, the generated carbon radical can readily desorb from the V_O-free surface because of its small adsorption energy, and, thus, can dimerize to form the coupling products. By contrast, on the V_O-rich surface, furfural prefers to adsorb on V_O with the oxygen atom of the carbonyl group filling the V_O site. Such configuration makes the generation of a confined alkoxy radical (CH–O•) energetically favourable (−1.25 eV) on the attack of $e^- + H^+$, whereas the formation of a •C–OH radical is endothermic (FIG. 6c). Therefore, furfural tends to undergo a two-step hydrogenation to deliver the alcohol product. In short, this research provides a molecular-level understanding on modulating product selectivity for furfural conversion by forming particular radical intermediates on the catalyst surface.

With these understandings in mind, for bioplatforms, the desired product can be altered by simply changing the catalyst used. Over V_O-rich A-sheet catalyst, in addition to furfural, 5-methyl furfural and vanillin derived from cellulose and lignin, respectively, can be converted into their corresponding alcohols, which are useful chemicals with high yields (>75%). On the other hand, these substrates can be transformed into corresponding C–C coupling products with yields ≥80% over R-rod catalyst. A selective radical coupling process of furfural over a $ZnIn_2S_4$ photocatalyst is also possible[43]. These chain-elongated products are regarded as valuable jet fuel precursors, as mentioned above.

Extraneous radical-induced lignin bond cleavage. In the above systems, the conversion processes always begin with the activation of biomass substrates into specific radicals, such as the first formation of C_β radical or alkoxy radical in the lignin *β*-O-4 bond cleavage. However, for the cleavage of more robust lignin linkages, these strategies would become inefficient. For example, the lignin 4-O-5 linkage (diaryl ether structure) is rather resistant to cleavage due to its high BDE (~75 kcal mol^{-1})[44–46] and it is hard to produce any radical species that can promote the targeted bond cleavage on stimulation of photo-generated carriers. In this context, introducing an active external radical species would be an alternative strategy to activate the robust structure, and, thus, achieve conversion.

An aryl carboxylic radical-mediated acidolysis strategy was adopted to cleave the aryl ether bond of the lignin 4-O-5 linkage under blue LEDs irradiation[45] (FIG. 7a). An acridinium photocatalyst that possesses a strong oxidative ability was used to generate the aryl carboxylic radical ($E^{4\text{-}CH3PhCO2\bullet/4\text{-}CH3PhCO2-}$ = +1.45 V versus SCE). Subsequently, the electrophilic radical species attacked the electron-rich aryl ring of the substrate to yield a metastable intermediate. Then, a Lewis acid catalyst, $Cu(TMHD)_2$, was used to coordinate and stabilize this intermediate and, more importantly, to promote C–O bond cleavage through a SET process with reduced photocatalyst to afford the final ester and phenol products. A sequential hydrolysis procedure can readily transform the benzoate ester into another molecule of phenol and recover the benzoate. By this method, the lignin 4-O-5 model substrate can be converted into phenol with high efficiency (80% yield) in a gram-scale flow reaction.

Generally, the fragmentation of the lignin *β*-O-4 linkage affords phenolic products[48]. Obtaining non-phenolic aromatics, such as valuable arylamine, would extend the application of lignin conversion; however, it requires the selective cleavage of a robust aryl C–O bond in the presence of a weaker aliphatic ether bond. To overcome this challenge, an intramolecular substitution method was developed to cleave the aryl C–O bond in the lignin *β*-O-4 linkage by using an installed nitrogen radical[47] (FIG. 7b). Prior to conversion, an acyl oxime moiety was introduced into the lignin *β*-O-4 linkage as the radical precursor. Thereby, reducing the modified compound by photoexcited phenothiazine catalyst would generate the key iminyl radical, which preferentially attacks the aryl C–O bond to form a spiro intermediate. After bond cleavage, primary arylamine and α-hydroxy ketone can be attained via further reduction and hydrolysis. By virtue of such an additionally installed iminyl radical, nitrogen-modified lignin model can be converted into methoxyl aniline and *β*-hydroxyl acetophenone in yields of 70% and 80%, respectively. Notably, 1.9 wt% of substituted arylamines can be obtained from modified lignin after 365-nm LEDs irradiation for 8 h at room temperature. These studies illustrate that the use of an active extraneous radical may offer an opportunity to achieve challenging transformations that are thermodynamically unfavourable based on the solo activation of biomass substrate. However, a specific effort is needed to regulate the extraneous radical to undergo the target reaction.

Regulating radical intermediate conversion

Regulating the conversion of active radical intermediates is important for valuable chemical production from biomass, especially for those possessing multiple downstream conversion routes. In this section, we describe recent advanced strategies for the selective conversion of radical intermediates derived from different biomass components, including the C_α radical from the lignin *β*-O-4 linkage, ketyl radicals from bio-polyols and alkyl radicals from fatty acids. In these cases, the radical species are generated via their thermodynamically favourable pathways on stimulation of photo-generated carriers. However, the production of the desired product is considerably hindered by unwanted side reactions of the reactive intermediates. In this context, rational fabrication of catalytic systems to subtly tune the interactions between radical intermediates and catalysts is crucial to prevent the active species from reacting in an unregulated manner.

Reductive bond cleavage of C_α radical in the lignin β-O-4 linkage. The cleavage of the *β*-O-4 linkage — the most abundant in natural lignin — is of great importance for lignin depolymerization[4]. The first

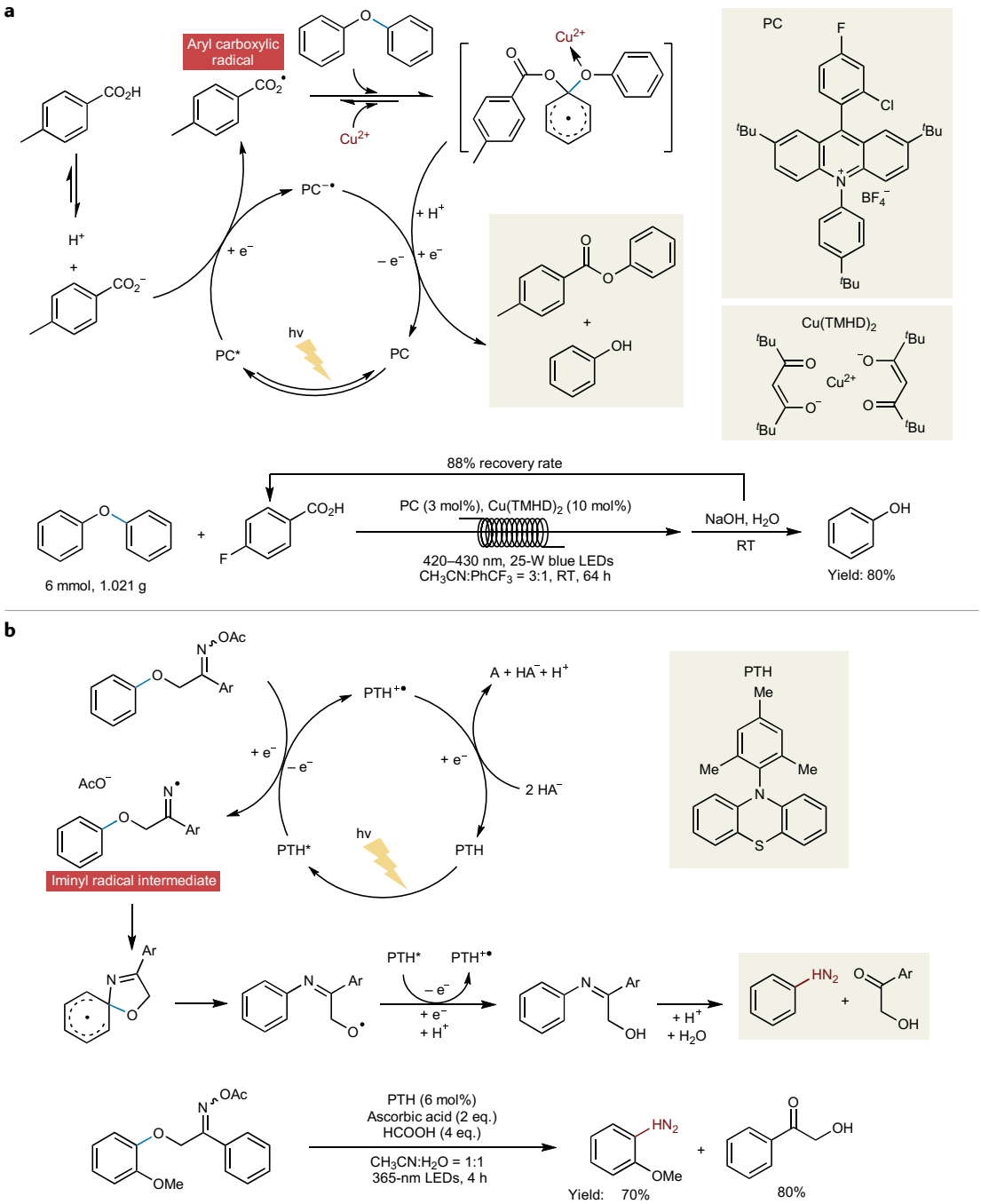

Fig. 7 | **Active external radical species induce lignin bond cleavage. a** | Aryl carboxylic radical-mediated acidolysis strategy to cleave the aryl C–O bond of the lignin 4-O-5 linkage. The bond scission is achieved by the electrophilic attack of the generated aryl carboxylic radical with the aid of a copper catalyst[45]. **b** | Photocatalytic aryl C–O bond cleavage in N-modified lignin β-O-4 linkage via an iminyl radical-induced intramolecular substitution. The excited phenothiazines (PTH) reduce the α-oximated lignin model to deliver the key iminyl radical, which subsequently induces the aryl C–O bond cleavage via intramolecular substitution[47]. LED, light-emitting diode; PC, photocatalyst; RT, room temperature. Panel **a** is adapted from REF.[45], CC BY 4.0. Panel **b** adapted with permission from REF.[48], American Chemical Society.

formation of a C_α radical via C_α–H bond activation is the most thermodynamically favourable on oxidation by holes. Generally, it would be successively oxidized to the ketone counterpart, which results in a decrease of the BDE of the C_β–O bond from 55 to 47 kcal mol^{-1}, making the subsequent reductive bond cleavage easier[49]. Such a tandem oxidation–reduction strategy has stimulated the development of numerous catalytic systems[50–52]. For instance, Pd/$ZnIn_2S_4$ can catalyse the aerobic oxidation of C_α–OH of lignin β-O-4 alcohols to offer the corresponding ketone under 455-nm light irradiation. Subsequently, a TiO_2–NaOAc system can be used to reductively cleave the C_β–O bond under 365-nm light irradiation[53]. Such stepwise photocatalytic degradation

Oxidation by holes
(Also known as hole-induced oxidation). Oxidation reaction triggered by photo-generated holes.

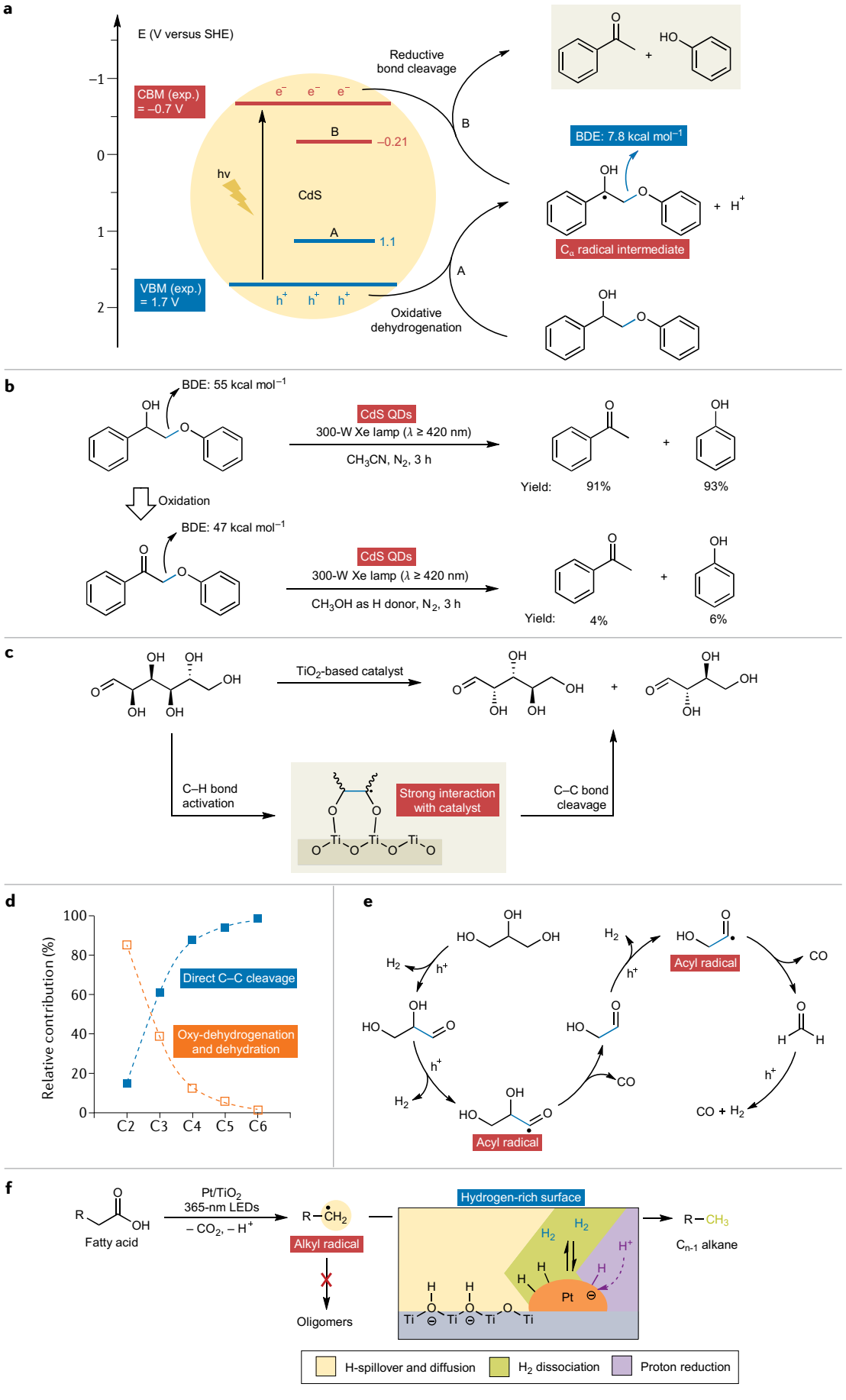
a
E (V versus SHE)
CBM (exp.) = –0.7 V
VBM (exp.) = 1.7 V
B
–0.21
CdS
A
1.1
hv
Reductive bond cleavage
Oxidative dehydrogenation
BDE: 7.8 kcal mol–1
Cα radical intermediate
b
BDE: 55 kcal mol–1
CdS QDs
300-W Xe lamp (λ ≥ 420 nm)
CH3CN, N2, 3 h
Yield: 91%
93%
Oxidation
BDE: 47 kcal mol–1
CdS QDs
300-W Xe lamp (λ ≥ 420 nm)
CH3OH as H donor, N2, 3 h
Yield: 4%
6%
c
TiO2-based catalyst
C–H bond activation
Strong interaction with catalyst
C–C bond cleavage
d
Relative contribution (%)
Direct C–C cleavage
Oxy-dehydrogenation and dehydration
C2
C3
C4
C5
C6
e
Acyl radical
CO
CO + H2
f
Pt/TiO2
365-nm LEDs
– CO2, – H+
Fatty acid
Alkyl radical
Oligomers
Hydrogen-rich surface
Cn-1 alkane
H-spillover and diffusion
H2 dissociation
Proton reduction

◀ Fig. 8 | **Regulating the conversion of radical intermediates derived from lignin, polyol molecules and fatty acids. a** | Photocatalytic C_β–O bond cleavage in the lignin β-O-4 linkage via electron–hole coupled mechanism. A photo-generated hole oxidizes the lignin substrate to furnish the C_α radical intermediate, which markedly weakens the C_β–O bond. Reducing the C_α radical by a photo-generated electron leads to the targeted C–O bond scission[17]. **b** | Photocatalytic conversion of the β-O-4 lignin model and pre-oxidized counterpart over CdS quantum dots (QDs)[17]. **c** | Photocatalytic low-carbon-number aldose production from glucose over TiO_2-based catalysts[71]. **d** | Relative contributions of direct C–C-cleavage and indirect conversion pathways (oxy-dehydrogenation and dehydration) for photocatalytic conversion of C2–C6 polyols over Rh/TiO_2 (REF.[82]). **e** | Photoforming glycerol into syngas via stepwise decarbonylation over [SO_4]/CdS. Acyl radicals are generated as key intermediates via sequential proton-coupled electron transfer processes over [SO_4]/CdS under irradiation and then undergo decarbonylation to produce CO (REF.[84]). **f** | Photocatalytic decarboxylation of fatty acids over hydrogen-rich Pt/TiO_2 surface. Electron-induced proton reduction, H_2 dissociation on Pt nanoparticles and H-spillover onto TiO_2 together form a hydrogen-rich surface for rapid hydrogen termination of generated radicals[91]. BDE, bond dissociation enthalpy; CBM, conduction band minimum; LED, light-emitting diode; SHE, standard hydrogen electrode; VBM, valence band maximum. Panel **a** adapted with permission from REF.[17], Springer Nature Limited. Panel **d** adapted with permission from REF.[82], Elsevier. Panel **f** adapted from REF.[91], Springer Nature Limited.

of lignin β-O-4 models can also be achieved by using two carbazolic co-polymer photocatalysts synthesized by co-polymerization of a carbazolic electron donor and an electron acceptor in a specified ratio[54]. Generally, this stepwise method necessitates an extra amount of oxidants or reductants in each step. Only a few cases can integrate the tandem oxidative and reductive reactions into one single catalytic system[55–57].

Actually, the C_α radical intermediate itself possesses a remarkably lower BDE of the C_β–O bond (7.8 kcal mol^{-1}) than that of the ketone counterpart, which implies a more effective pathway for lignin β-O-4 linkage fragmentation if the photo-generated electron can access the radical intermediate before its successive oxidation. An electron–hole coupled (EHCO) method was developed for the efficient fragmentation of the β-O-4 bond in lignin models over a CdS quantum dots (QDs) photocatalyst[17] (FIG. 8a,b). The key step is the electron-induced reductive cleavage of the C_β–O bond in the C_α radical intermediate, which yields ketones and phenols as final products. The reductive potential for this process is −0.21 V versus standard hydrogen electrode, which is higher than the conduction band minimum (CBM) of CdS (−0.7 V versus standard hydrogen electrode). Such a large overpotential indicates that the electron from excited CdS can readily transfer to the C_α radical, and, hence, induce the bond cleavage reaction. The deposition of Ni onto CdS can alter its inherent band structure by forming a Mott–Schottky junction, which would dominantly catalyse the dehydrogenation of the lignin β-O-4 model to deliver the ketone intermediate, rather than the C_α radical-mediated bond scission[56]. Meanwhile, conversion of the ketone counterpart is extremely slow over CdS QDs photocatalyst due to its relatively high energy barrier for reductive bond cleavage. These results demonstrate that the suitable band structure of CdS plays a crucial role in the C_α radical-mediated bond scission process. Moreover, the CdS QDs with a hydrophilic ligand (3-mercaptopropionic acid) can be homogeneously solubilized in the reaction solvent, which enables its application in the direct conversion of native birch woodmeal[17]. Under visible light irradiation, the lignin component was decomposed into monomeric aromatics via β-O-4 linkage cleavage with a high yield of 26.7 wt% (close to the theoretical maximum yield). In addition, the carbohydrates can be well preserved (>90%), separated after the reaction and readily converted into xylose and glucose via an acidolysis or enzymolysis process, representing the full use of lignocellulose under mild conditions. In a latter study, the important role of the organic ligand chelated on CdS QDs was further investigated in detail[58]. Transient absorption dynamics analysis and electrochemical characterizations reveal that the ligands not only help to disperse QDs to form colloidal solution — which enables the intimate contact between the catalyst and the lignin substrate — but also mediate electron transfer between CdS QDs and the substrate through an electron-tunnelling process. This is pivotal to the sequential participation of photo-generated hole and electron in the EHCO mechanism. Ag^+-exchanged CdS nanoparticles show enhanced photocatalytic activity for lignin β-O-4 bond cleavage via a similar mechanism[59]. In comparison with metal deposition, Ag^+ exchange does not alter the intrinsic band structure of CdS considerably, and, instead, it downshifts the Fermi level of CdS, accelerates the separation of photo-generated carriers and strengthens the proton affinity of catalyst, which is beneficial to the EHCO transfer process.

The importance of the energy band structure of the photocatalyst for the C_α radical-mediated bond cleavage in the β-O-4 linkage was further demonstrated in a latter study[60]. A series of $Zn_mIn_2S_{m+3}$ catalysts were synthesized, in which their energy band structures can be easily tuned by varying the Zn/In ratios. As the *m* value increases from 1 to 6, the VBM of $Zn_mIn_2S_{m+3}$ shifts to more positive values, from 1.65 to 1.99 V, whereas the CBM shifts in the opposite direction, from −0.47 to −0.61 V. In the EHCO mechanism, cleavage of the β-O-4 bond necessitates the participation of both photo-generated hole and electron, that is, their direct interactions with the lignin substrate to produce the key C_α radical and drive its subsequent conversion. Therefore, $Zn_6In_2S_9$ with the most positive VBM and the most negative CBM showed the highest activity for lignin β-O-4 model conversion under 395-nm light irradiation because of its strongest oxidative and reductive ability among the synthesized catalysts.

Similarly, the formation of another C_α radical from dehydroxylation in the lignin β-O-4 linkage would also decrease the BDE of the C_β–O bond to ~16 kcal mol^{-1}, thereby, the subsequent bond scission reaction would be rather facile. In previous research, a relatively high temperature (180 °C) was required to produce this radical from dehydroxylation, allowing the bond scission to dramatically compete with a range of side reactions[61]. However, this process has not yet been achieved by photocatalytic methods. Therefore, if the desired C_α radical can be selectively generated over a suitable photocatalyst under mild conditions, this dehydroxylation–reduction protocol would be an efficient approach for lignin depolymerization, offering a chance to access valuable alkylphenol products.

Mott–Schottky junction
Refers to the metal–semiconductor junction that possesses an in-built potential energy barrier (Schottky barrier). This barrier allows electrons to transfer from the semiconductor to the metal but blocks the transfer process in the opposite direction.

Carbon-radical-mediated C–C bond cleavage in polyol molecules. As the largest fraction of biomass, carbohydrates (cellulose and hemicellulose) hold great potential for biomass use on a large scale[40]. Through enzymatic or acid hydrolysis, they can be readily decomposed into a series of disaccharides and monosaccharides, such as glucose and fructose. In addition, glycerol is generated as a by-product during biodiesel production, accounting for about one-tenth of the mass of biodiesel, hence, value-added use of glycerol also represents an important topic for biomass conversion[62,63]. Unlike the relatively firm structure of lignin, the inherent polyhydroxylated structures and the consequential low oxidation potential render carbohydrates and glycerol vulnerable to hole-induced oxidation[64]. Therefore, these polyols have been intensively used as sacrificial agents to rapidly consume the photo-generated hole and, thereby, enhance the electron-induced H_2 evolution. In 1980, sugars and cellulose were first reported to reform into H_2 and CO_2 over RuO_2/TiO_2/Pt photocatalyst under Xe lamp irradiation[65]. Since then, a great number of photocatalytic systems have been developed for H_2 production from bio-polyols[66–68]. However, the biomass components are dominantly degraded into CO_2 with a trivial amount of carbonic intermediates. For instance, less than 0.2% of gaseous methanol and ethanol was generated in the above example[65]. In another case, a considerable amount of formate was observed in the photo-reforming of various carbohydrates over a CdS/CdO_x QDs photocatalyst[69]. Similarly, under UV irradiation, a 35% yield of formate can be attained from glucose over a TiO_2 catalyst in an alkaline aqueous solution, but more than 60% of substrate was inevitably degraded into CO_2 (REF.[70]).

Several photocatalytic systems have still been developed for selective carbonic chemical production from bio-polyols degradation. For instance, glucose can be converted into arabinose and erythrose via C_1–C_2 bond cleavage (α-scission) with a total selectivity of 91% at 65% conversion over Rh/rutile TiO_2 photocatalyst[71]. The generation of peroxy species with a relatively gentle oxidative ability is vital to the high selectivity. In a latter case, a LMCT effect was used to achieve selective glucose conversion over TiO_2 catalyst under visible light irradiation[72]. The TiO_2–glucose LMCT complex can be activated under visible light irradiation, thereby, stepwise degrading glucose into low-carbon-number aldoses in high selectivity. Under optimal conditions, a high total selectivity of C_2–C_5 aldoses (93%) can be obtained at 42% glucose conversion with a minor selectivity of gluconic acid (7%).

During these processes, the photo-generated hole firstly activates the C–H bond to generate the corresponding ketyl radicals; the subsequent C–C bond scission is the key step to deliver low-carbon-number aldoses. It is noteworthy that, in the thermal dissociation process, polyols (for example, ethylene glycol (EG) at >400 K) first undergo dehydration and dehydrogenation reactions[73]. Next, the ketyl radical readily transforms into the corresponding aldehyde or ketone through either a successive oxidation reaction or a spontaneous electron donation to the conduction band of a semiconductor photocatalyst. The latter process is generally termed 'current doubling'[74,75]. In addition, the ketyl radical could also dehydrate and subsequently isomerize into a secondary carbon radical[76]. This pathway is more prominent in an acidic aqueous solution. Therefore, the ketyl-radical-mediated C–C bond cleavage reaction in the above-mentioned systems is quite unique and closely related to the interactions between polyol molecule and semiconductor photocatalyst (for example, TiO_2) (FIG. 8c). The intimate chelation between hydroxyl groups of polyol and surface Ti(IV) sites has been evidenced by titanium K-edge X-ray absorption near edge structure spectra and infrared spectroscopic studies[77,78]. By using scanning tunnelling microscopy analysis, the EG adsorption on the Ti_{5c} sites of rutile TiO_2(110) surface and its light-induced C–C bond cleavage can be directly observed[79]. The EG molecule is inferred to interact with the catalyst surface with two oxygen atoms bound to two neighbouring metal ions. Detailed investigation reveals that the C–C bond scission is the only pathway for EG photoconversion over TiO_2 under deaerated conditions. Computational studies also demonstrate that glucose is favourable thermodynamically to adsorb on TiO_2 via bidentate binding mode involving the vicinal hydroxyl groups. The highest occupied molecular orbital of this surface complex is dominantly localized on the glucose molecule, making adsorbed glucose vulnerable to photo-oxidation[80]. More importantly, the oxo bridges between chemisorbed carbohydrate and metal oxide surface confine the hole-induced ketyl radical to some extent, suppress its rapid dehydration and successive oxidation and facilitate its C–C bond cleavage with the elimination of a formyl radical[81]. By combining electron paramagnetic resonance and isotope substitution, studies indicated the preferential C–H bond activation on carbon-1, carbon-2 and carbon-3 sites of adsorbed carbohydrates by photo-generated holes, whereas C–C bond fragmentation always initiates with the terminal carbon. This implies a very interesting stepwise C–C bond scission strategy for bio-polyol upgrading.

By analysing the rate constants from kinetic modelling and initial selectivity of primary products, oxidative C–C bond scission is shown as the dominant pathway for glycerol photo-reforming over Rh/TiO_2 catalyst — accounting for 61% of initial glycerol conversion — whereas oxidations of primary and secondary carbon into glyceraldehyde and dihydroxyacetone only represent minor reaction channels (26% and 13%, respectively)[82] (FIG. 8d). More interestingly, the polyol structure significantly influences its photoconversion pathways, and the C–C bond rupture would become progressively dominant with the increasing polyol carbon chain. For instance, 98% of sorbitol preferentially undergoes C–C bond fragmentation on hole-induced oxidation. Moreover, using time-resolved transient absorption spectroscopy, polyol with more hydroxyl groups is revealed to have a dramatically higher hole scavenging efficiency over TiO_2 (REF.[77]). These results further demonstrate the vital role of the interactions between polyol and catalyst in the photo-oxidation process. That is, polyol with more anchoring hydroxyl groups would remarkably strengthen its physisorption and chemisorption on the catalyst surface, which not only accelerates

the electron transfer process to initiate the reaction but also confines the ketyl radical intermediate more efficiently, thus, altering its dominant conversion pathway from dehydrogenation through successive oxidation or current doubling process to the C–C bond scission reaction.

The –CHOH– moiety is the basic unit of bio-polyols. Sequential cleavage of the interunit C–C bonds would fragment polyols into important C1 chemicals, such as methanol, formic acid and CO. TiO_2 nanorod catalysts with copper deposition (Cu/TNR) were synthesized that can efficiently transform various bio-polyols into methanol and syngas under UV irradiation[83]. For instance, under optimal conditions, glycerol can be reformed into about 40% yield of methanol, along with 31% yield of CO_2, 3.6% yield of CO and H_2 (22 mmol g_{cat}^{-1}) after 365-nm LEDs (18 W) irradiation for 12 h at room temperature. The V_O on Cu/TNR catalysts plays an important role in the polyol fragmentation. Density functional theory calculations reveal that EG, a simple but representative polyol molecule, tends to dissociatively adsorb on V_O with an adsorption energy of −1.75 eV, while its dissociative adsorption on perfect TiO_2(110) surface is endothermic (0.33 eV). Therefore, the stronger interaction between the polyol molecule and defective catalyst surface would significantly promote the substrate activation and the subsequent C–C bond cleavage, as mentioned above. As a result, Cu/TNR is at least three times more active than a Cu/P25 catalyst with a negligible amount of V_O for glycerol conversion (methanol yield 28.9% versus 9.4%). Meanwhile, no methanol can be attained from 1,3-propanediol, 1-propanol or 2-propanol conversion. These results demonstrate a defect-promoted mechanism for C–C bond cleavage in vicinal diol structure.

The photo-reforming processes over TiO_2-based catalysts usually involve the ketyl-radical-mediated C–C bond cleavage reaction. However, only a few systems are able to attain carbonic chemicals from polyols with acceptable selectivity, especially at relatively high conversion; the unselective mineralization reactions that eventually produce CO_2 seem inevitable. In the above-mentioned case[83], copper deposition was indispensable for C1 chemical production. Although the generated methanol would be successively oxidized into formic acid over a prolonged reaction time, decreasing the copper loading would lead to selectively degrading formic acid into CO instead of CO_2. Therefore, simply changing the reaction conditions and copper loading on catalysts can alter the major product from methanol into syngas ($CO + H_2$). For instance, after a pre-hydrogenolysis procedure, cellulose can be transformed into 45% yield of CO over a Cu/TNR catalyst with 0.1 wt% copper loading. In addition, lowering the water concentration can markedly suppress the production of CO_2, as it can restrain the generation of highly oxidative hydroxyl radicals. Similarly, the generation of peroxy species is beneficial to selective aldose production from glucose, while the participation of hydroxyl radicals would lead to a low selectivity[71]. Consequently, we can conclude that regulating the conversion of secondary intermediates derived from the C–C bond scission is also important for selective carbonic chemical production from bio-polyols.

It should be noted that ketyl-radical-mediated C–C bond cleavage is not the only pathway for bio-polyols use by photocatalysis. Very recently, a CdS catalyst with surface sulfate ion decoration ($[SO_4]$/CdS) was reported to selectively transform various sugars and glycerol into a syngas mixture under visible light irradiation[84]. The hole-induced ketyl radical from glycerol would be successively oxidized to glyceraldehyde over $[SO_4]$/CdS instead of undergoing C–C bond cleavage due to the relatively weaker interaction between the substrate and the sulfide surface than that over TiO_2-based catalysts (FIG. 8e). Subsequently, glyceraldehyde would generate acyl radical via a PCET process over $[SO_4]$/CdS, which then undergoes a decarbonylation reaction to deliver glycolaldehyde and CO. Glycolaldehyde is eventually transformed into CO and H_2 via two sequent acyl-radical-mediated decarbonylation processes. As such, under blue LEDs (60 W) irradiation, glycerol can be decomposed into syngas over $[SO_4]$/CdS with a high CO generation rate of 0.31 mmol g_{cat}^{-1} h^{-1}, and, remarkably, no CO_2 was generated.

Rapid hydrogenation of alkyl radicals derived from fatty acid decarboxylation. Many fatty acids can be harvested from wood, crops, animals and algae cultivation[85]. Owing to their abundance, easy accessibility and inherent structural similarities to diesel-type hydrocarbons, they are regarded as promising feedstock for renewable diesel and jet fuel production; however, relatively harsh conditions (reaction temperatures ≥250 °C, H_2 pressures ≥2 MPa) are generally needed to transform them into hydrocarbon fuels in thermocatalysis[85,86]. Alternatively, through a SET process, fatty acids can be oxidized to the corresponding carboxyl radical, which rapidly loses CO_2 and yields an alkyl radical[87]. The subsequent conversion of this radical intermediate determines the product distribution, whereby its hydrogen termination would ideally produce a suitable carbon number alkane for diesel and jet fuel applications. However, such a process is dramatically challenged by the active nature of radical species. The alkyl radicals tend to dimerize via C–C coupling, and they can be further oxidized to the corresponding cations, eventually transforming into a range of products, such as ether, ester and oligomers[88–90]. Therefore, regulating the alkyl radical conversion is vital for desired alkane production from fatty acid decarboxylation.

Various fatty acids can be efficiently converted into corresponding C_{n-1} alkanes with high yields (≥90%) via photocatalytic decarboxylation over Pt/TiO_2 catalyst under mild conditions (ambient temperature, $p_{H2} \leq 0.2$ MPa)[91]. In this case, a hydrogen-rich catalyst surface is constructed by the interactions between the catalyst and H_2 to modulate the alkyl radical conversion for preferential hydrogenation (FIG. 8f). H_2 can be readily activated and dissociate on the highly dispersed Pt nanoparticles, and subsequently spill over onto TiO_2 support. Hence, once the alkyl radical is generated from substrate decarboxylation, it would be rapidly terminated by hydrogen in such a hydrogen-rich circumstance to

yield desired C_{n-1} alkane, thereby, suppressing unwanted side reactions. For instance, *n*-undecane can be attained in 93% yield from lauric acid in a H_2 atmosphere. In sharp contrast, the yield dropped to 59% when changing the reaction atmosphere to Ar. It is notable that the photo-generated electrons can reduce protons to compensate for the continuous consumption of surface hydrogen by the hole-induced alkyl radicals, so such a redox neutral mechanism indicates a minimal net H_2 consumption during the reaction. Moreover, this method can be applied to the conversion of soybean fatty acids and tall oil fatty acids, the low-value by-products from soybean oil refinery and the pulp industry, respectively. These fatty acid mixtures can be smoothly converted into corresponding alkanes in high yields (up to 95%) under optimal conditions after a facile pre-hydrogenation procedure.

Summaries and perspectives

In this Review, we have demonstrated that photocatalysis is an attractive and valid pathway for valuable chemical production from various biomass components. In particular, active and energetic light-induced radical intermediates provide unique reaction patterns for selective biomass upgrading; however, fine control of the generation and subsequent conversion of these reactive species is imperative for high efficiency. For future studies, a focus to develop more efficient catalytic systems is still highly beneficial. Exploration devoted to the subtle conversion of radical intermediates is encouraged, as their special structures with unpaired electrons and the resulting impact on the surrounding chemical bonding would provide new chemistry beyond conventional thermocatalysis, especially with the further participation of a photo-generated hole/electron. One example is the EHCO mechanism for lignin fragmentation[17]; the photo-generated hole activates the lignin substrate into a C_α radical with a remarkably weakened C_β–O bond (BDE = 7.8 kcal mol^{-1}) and the photo-generated electron induces its sequent reductive bond cleavage. Moreover, the introduction of suitable extraneous radical species represents great potential not only to initiate challenging conversions but also to mediate the direct reactions between biomass macromolecules and heterogeneous photocatalysts. In addition, fundamental research into the interactions between photocatalysts and highly functionalized biomass components and the corresponding transient radical intermediates is important to provide molecular-level guidance for the design of advanced catalysts and the optimization of reaction parameters[92], which necessitates time-resolved and/or operando techniques and theoretical simulation. As the key mediators that bridge the photoexcited catalysts and the final products, the reactions of the active radical species directly determine the efficiency of biomass use and, thus, deserve serious consideration for the design of new catalytic systems in the future.

Despite the continuous progress in photocatalytic biomass conversion, most of the current systems are still at the laboratory scale and far from practical use. Raw lignocellulose is an arguably viable feedstock for large-scale biomass valorization, although pretreatment is generally needed to fractionate carbohydrates (cellulose and hemicelluloses) and lignin, because different components require distinct conversion strategies[93]. In addition, the structures of obtained fractions vary dramatically with different lignocellulose sources and pretreatment techniques[4], which brings great challenges for the subsequent photocatalytic conversion. For instance, most of the established methods focus on maximizing the production of carbohydrates and lead to the formation of recondensed lignin structures that are resistant to downstream conversion[94,95]. Moreover, impurities in raw biomass (for example, nitrogen, sulfur and metal ions) may negatively impact the radical reactions in photocatalysis[5,63]. Therefore, a pretreatment methodology to deliver high-quality fractions with required purities is the prerequisite for efficient valorization of raw biomass. Furthermore, given the structural complexity and macromolecular nature of biomass feedstocks, integrating photocatalysis with other physical, biological and chemical techniques would offer great opportunities to achieve full conversion of biomass, making its practical use more feasible[1,17,83]. In addition, techno-economic analysis and life-cycle assessment are helpful to provide overall prediction and assessment on the technical feasibility, profitability and sustainability footprint for large-scale biomass valorization by photocatalysis[96,97]. At the current stage, to establish an efficient photocatalytic system with high energy-converting efficiency, high productivity and long-term stability is of fundamental priority before considering the scale-up application.

Published online: 10 February 2022

1. Liao, Y. et al. A sustainable wood biorefinery for low-carbon footprint chemicals production. *Science* **367**, 1385–1390 (2020).
2. Amidon, T. E. & Liu, S. Water-based woody biorefinery. *Biotechnol. Adv.* **27**, 542–550 (2009).
3. Deneyer, A. et al. Direct upstream integration of biogasoline production into current light straight run naphtha petrorefinery processes. *Nat. Energy* **3**, 969–977 (2018).
4. Li, C., Zhao, X., Wang, A., Huber, G. W. & Zhang, T. Catalytic transformation of lignin for the production of chemicals and fuels. *Chem. Rev.* **115**, 11559–11624 (2015).
5. Granone, L. I., Sieland, F., Zheng, N., Dillert, R. & Bahnemann, D. W. Photocatalytic conversion of biomass into valuable products: a meaningful approach? *Green Chem.* **20**, 1169–1192 (2018).
6. Liu, X., Duan, X., Wei, W., Wang, S. & Ni, B.-J. Photocatalytic conversion of lignocellulosic biomass to valuable products. *Green Chem.* **21**, 4266–4289 (2019).
7. Wu, X. et al. Photocatalytic transformations of lignocellulosic biomass into chemicals. *Chem. Soc. Rev.* **49**, 6198–6223 (2020).
This is an up-to-date and comprehensive review on photocatalytic conversion of lignocellulosic biomass.
8. Luo, N. et al. Visible-light-driven coproduction of diesel precursors and hydrogen from lignocellulose-derived methylfurans. *Nat. Energy* **4**, 575–584 (2019).
9. Zhang, C. & Wang, F. Catalytic lignin depolymerization to aromatic chemicals. *Acc. Chem. Res.* **53**, 470–484 (2020).
10. Recupero, F. & Punta, C. Free radical functionalization of organic compounds catalyzed by N-hydroxyphthalimide. *Chem. Rev.* **107**, 3800–3842 (2007).
11. Wu, X. et al. Selectivity control in photocatalytic valorization of biomass-derived platform compounds by surface engineering of titanium oxide. *Chem* **6**, 3038–3053 (2020).
This paper shows that regulating the interactions between substrate and catalyst by surface engineering can selectively activate furfural into an oxygen or carbon radical intermediate.
12. Yi, H. et al. Recent advances in radical C–H activation/radical cross-coupling. *Chem. Rev.* **117**, 9016–9085 (2017).
13. Xie, J., Jin, H. & Hashmi, A. S. K. The recent achievements of redox-neutral radical C–C cross-coupling enabled by visible-light. *Chem. Soc. Rev.* **46**, 5193–5203 (2017).
14. Gao, Z., Luo, N., Huang, Z., Taylor, S. H. & Wang, F. Controlling radical intermediates in photocatalytic conversion of low-carbon-number alcohols. *ACS Sustain. Chem. Eng.* **9**, 6188–6202 (2021).
15. Yayla, H. G., Wang, H., Tarantino, K. T., Orbe, H. S. & Knowles, R. R. Catalytic ring-opening of cyclic alcohols enabled by PCET activation of strong O–H bonds. *J. Am. Chem. Soc.* **138**, 10794–10797 (2016).
16. Ota, E., Wang, H., Frye, N. L. & Knowles, R. R. A redox strategy for light-driven, out-of-equilibrium isomerizations and application to catalytic C–C bond

cleavage reactions. *J. Am. Chem. Soc.* **141**, 1457–1462 (2019).
17. Wu, X. et al. Solar energy-driven lignin-first approach to full utilization of lignocellulosic biomass under mild conditions. *Nat. Catal.* **1**, 772–780 (2018).
This paper reports a photoredox electron–hole coupled protocol for lignin *β*-O-4 bond cleavage.
18. Wang, Y., Liu, Y., He, J. & Zhang, Y. Redox-neutral photocatalytic strategy for selective C–C bond cleavage of lignin and lignin models via PCET process. *Sci. Bull.* **64**, 1658–1666 (2019).
19. Mayer, J. M., Hrovat, D. A., Thomas, J. L. & Borden, W. T. Proton-coupled electron transfer versus hydrogen atom transfer in benzyl/toluene, methoxyl/methanol, and phenoxyl/phenol self-exchange reactions. *J. Am. Chem. Soc.* **124**, 11142–11147 (2002).
20. Nguyen, S. T., Murray, P. R. D. & Knowles, R. R. Light-driven depolymerization of native lignin enabled by proton-coupled electron transfer. *ACS Catal.* **10**, 800–805 (2020).
21. Zhou, W., Nakahashi, J., Miura, T. & Murakami, M. Light/copper relay for aerobic fragmentation of lignin model compounds. *Asian J. Org. Chem.* **7**, 2431–2434 (2018).
22. Gazi, S. et al. Selective photocatalytic C–C bond cleavage under ambient conditions with earth abundant vanadium complexes. *Chem. Sci.* **6**, 7130–7142 (2015).
23. Gazi, S. et al. Kinetics and DFT studies of photoredox carbon–carbon bond cleavage reactions by molecular vanadium catalysts under ambient conditions. *ACS Catal.* **7**, 4682–4691 (2017).
24. Liu, H., Li, H., Luo, N. & Wang, F. Visible-light-induced oxidative lignin C–C bond cleavage to aldehydes using vanadium catalysts. *ACS Catal.* **10**, 632–643 (2020).
25. Wang, Y., He, J. & Zhang, Y. $CeCl_3$-promoted simultaneous photocatalytic cleavage and amination of C_α–C_β bond in lignin model compounds and native lignin. *CCS Chem.* **2**, 107–117 (2020).
26. Hou, T. et al. Yin and Yang dual characters of CuO_x clusters for C–C bond oxidation driven by visible light. *ACS Catal.* **7**, 3850–3859 (2017).
27. Zhao, K. et al. Efficient water oxidation under visible light by tuning surface defects on ceria nanorods. *J. Mater. Chem. A* **3**, 20465–20470 (2015).
28. Liu, H. et al. Photocatalytic cleavage of C–C bond in lignin models under visible light on mesoporous graphitic carbon nitride through π–π stacking interaction. *ACS Catal.* **8**, 4761–4771 (2018).
29. Kang, Y. et al. Metal-free photochemical degradation of lignin-derived aryl ethers and lignin by autologous radicals through ionic liquid induction. *ChemSusChem* **12**, 4005–4013 (2019).
30. Wang, M. et al. Acid promoted C–C bond oxidative cleavage of β-O-4 and β-1 lignin models to esters over a copper catalyst. *Green Chem.* **19**, 702–706 (2017).
31. Ma, L., Zhou, H., Kong, X., Li, Z. & Duan, H. An electrocatalytic strategy for C–C bond cleavage in lignin model compounds and lignin under ambient conditions. *ACS Sustain. Chem. Eng.* **9**, 1932–1940 (2021).
32. Cui, T. et al. Atomically dispersed $Pt–N_3C_1$ sites enabling efficient and selective electrocatalytic C–C bond cleavage in lignin models under ambient conditions. *J. Am. Chem. Soc.* **143**, 9429–9439 (2021).
33. Have, R. T. & Teunissen, P. J. M. Oxidative mechanisms involved in lignin degradation by white-rot fungi. *Chem. Rev.* **101**, 3397–3413 (2001).
34. Cho, D. W. et al. Nature and kinetic analysis of carbon–carbon bond fragmentation reactions of cation radicals derived from SET-oxidation of lignin model compounds. *J. Org. Chem.* **75**, 6549–6562 (2010).
35. Cho, D. W. et al. Regioselectivity of enzymatic and photochemical single electron transfer promoted carbon–carbon bond fragmentation reactions of tetrameric lignin model compounds. *J. Org. Chem.* **76**, 2840–2852 (2011).
36. Lim, S. H. et al. Effects of alkoxy groups on arene rings of lignin β-O-4 model compounds on the efficiencies of single electron transfer-promoted photochemical and enzymatic C–C bond cleavage reactions. *J. Org. Chem.* **78**, 9431–9443 (2013).
37. Tay, N. E. S. & Nicewicz, D. A. Cation radical accelerated nucleophilic aromatic substitution via organic photoredox catalysis. *J. Am. Chem. Soc.* **139**, 16100–16104 (2017).
38. Werpy, T. & Petersen, G. Top value added chemicals from biomass. Volume I — Results of screening for potential candidates from sugars and synthesis gas (US Department of Energy, 2004).
39. Bozell, J. J. & Petersen, G. R. Technology development for the production of biobased products from biorefinery carbohydrates — the US Department of Energy's "Top 10" revisited. *Green Chem.* **12**, 539–554 (2010).
40. Mika, L. T., Cséfalvay, E. & Németh, Á. Catalytic conversion of carbohydrates to initial platform chemicals: chemistry and sustainability. *Chem. Rev.* **118**, 505–613 (2017).
41. Shylesh, S., Gokhale, A. A., Ho, C. R. & Bell, A. T. Novel strategies for the production of fuels, lubricants, and chemicals from biomass. *Acc. Chem. Res.* **50**, 2589–2597 (2017).
42. Nakajima, M., Fava, E., Loescher, S., Jiang, Z. & Rueping, M. Photoredox-catalyzed reductive coupling of aldehydes, ketones, and imines with visible light. *Angew. Chem. Int. Ed.* **54**, 8828–8832 (2015).
43. Han, G., Liu, X., Cao, Z. & Sun, Y. Photocatalytic pinacol C–C coupling and jet fuel precursor production on $ZnIn_2S_4$ nanosheets. *ACS Catal.* **10**, 9346–9355 (2020).
44. Sun, Z., Fridrich, B., de Santi, A., Elangovan, S. & Barta, K. Bright side of lignin depolymerization: toward new platform chemicals. *Chem. Rev.* **118**, 614–678 (2018).
45. Tan, F.-F., He, X.-Y., Tian, W.-F. & Li, Y. Visible-light photoredox-catalyzed C–O bond cleavage of diaryl ethers by acridinium photocatalysts at room temperature. *Nat. Commun.* **11**, 6126 (2020).
This paper reports a strategy to use extraneous radical species to cleave C–O bonds in diaryl ethers.
46. Zeng, H., Cao, D., Qiu, Z. & Li, C.-J. Palladium-catalyzed formal cross-coupling of diaryl ethers with amines: slicing the 4-O-5 linkage in lignin models. *Angew. Chem. Int. Ed.* **57**, 3752–3757 (2018).
47. Li, H., Bunrit, A., Li, N. & Wang, F. Heteroatom-participated lignin cleavage to functionalized aromatics. *Chem. Soc. Rev.* **49**, 3748–3763 (2020).
48. Li, H. et al. Photocatalytic cleavage of aryl ether in modified lignin to non-phenolic aromatics. *ACS Catal.* **9**, 8843–8851 (2019).
49. Zhang, C. & Wang, F. Sell a dummy: adjacent functional group modification strategy for the catalytic cleavage of lignin β-O-4 linkage. *Chin. J. Catal.* **38**, 1102–1107 (2017).
50. Nguyen, J. D., Matsuura, B. S. & Stephenson, C. R. J. A photochemical strategy for lignin degradation at room temperature. *J. Am. Chem. Soc.* **136**, 1218–1221 (2014).
51. Magallanes, G. et al. Selective C–O bond cleavage of lignin systems and polymers enabled by sequential palladium-catalyzed aerobic oxidation and visible-light photoredox catalysis. *ACS Catal.* **9**, 2252–2260 (2019).
52. Yang, C., Kärkäs, M. D., Magallanes, G., Chan, K. & Stephenson, C. R. J. Organocatalytic approach to photochemical lignin fragmentation. *Org. Lett.* **22**, 8082–8085 (2020).
53. Luo, N. et al. Photocatalytic oxidation–hydrogenolysis of lignin β-O-4 models via a dual light wavelength switching strategy. *ACS Catal.* **6**, 7716–7721 (2016).
54. Luo, J., Zhang, X., Lu, J. & Zhang, J. Fine tuning the redox potentials of carbazolic porous organic frameworks for visible-light photoredox catalytic degradation of lignin *β*-O-4 models. *ACS Catal.* **7**, 5062–5070 (2017).
55. Luo, N. et al. Visible-light-driven self-hydrogen transfer hydrogenolysis of lignin models and extracts into phenolic products. *ACS Catal.* **7**, 4571–4580 (2017).
56. Han, G. et al. Highly selective photocatalytic valorization of lignin model compounds using ultrathin metal/CdS. *ACS Catal.* **9**, 11341–11349 (2019).
57. Chen, K., Schwarz, J., Karl, T. A., Chatterjee, A. & König, B. Visible light induced redox neutral fragmentation of 1,2-diol derivatives. *Chem. Commun.* **55**, 13144–13147 (2019).
58. Wu, X. et al. Ligand-controlled photocatalysis of CdS quantum dots for lignin valorization under visible light. *ACS Catal.* **9**, 8443–8451 (2019).
59. Yoo, H. et al. Enhancing photocatalytic β-O-4 bond cleavage in lignin model compounds by silver-exchanged cadmium sulfide. *ACS Catal.* **10**, 8465–8475 (2020).
60. Lin, J. et al. Visible-light-driven cleavage of C–O linkage for lignin valorization to functionalized aromatics. *ChemSusChem* **12**, 5023–5031 (2019).
61. Zhang, C. et al. Cleavage of the lignin β-O-4 ether bond *via* a dehydroxylation–hydrogenation strategy over a NiMo sulfide catalyst. *Green Chem.* **18**, 6545–6555 (2016).
62. Pagliaro, M., Ciriminna, R., Kimura, H., Rossi, M. & Della Pina, C. From glycerol to value-added products. *Angew. Chem. Int. Ed.* **46**, 4434–4440 (2007).
63. Yang, F., Hanna, M. A. & Sun, R. Value-added uses for crude glycerol–a byproduct of biodeisel production. *Biotechnol. Biofuels* **5**, 13 (2012).
64. Shimura, K. & Yoshida, H. Heterogeneous photocatalytic hydrogen production from water and biomass derivatives. *Energy Environ. Sci.* **4**, 2467–2481 (2011).
65. Kawai, T. & Sakata, T. Conversion of carbohydrate into hydrogen fuel by a photocatalytic process. *Nature* **286**, 474–476 (1980).
66. Schneider, J. et al. Understanding TiO_2 photocatalysis: mechanisms and materials. *Chem. Rev.* **114**, 9919–9986 (2014).
67. Puga, A. V. Photocatalytic production of hydrogen from biomass-derived feedstocks. *Coord. Chem. Rev.* **315**, 1–66 (2016).
68. Kuehnel, M. F. & Reisner, E. Solar hydrogen generation from lignocellulose. *Angew. Chem. Int. Ed.* **57**, 3290–3296 (2018).
69. Wakerley, D. W. et al. Solar-driven reforming of lignocellulose to H_2 with a CdS/CdO_x photocatalyst. *Nat. Energy* **2**, 17021 (2017).
70. Jin, B., Yao, G., Wang, X., Ding, K. & Jin, F. Photocatalytic oxidation of glucose into formate on nano TiO_2 catalyst. *ACS Sustain. Chem. Eng.* **5**, 6377–6381 (2017).
71. Chong, R. et al. Selective conversion of aqueous glucose to value-added sugar aldose on TiO_2-based photocatalysts. *J. Catal.* **314**, 101–108 (2014).
72. Da Vià, L., Recchi, C., Gonzalez-Yañez, E. O., Davies, T. E. & Lopez-Sanchez, J. A. Visible light selective photocatalytic conversion of glucose by TiO_2. *Appl. Catal. B* **202**, 281–288 (2017).
73. Li, Z., Kay, B. D. & Dohnálek, Z. Dehydration and dehydrogenation of ethylene glycol on rutile TiO_2(110). *Phys. Chem. Chem. Phys.* **15**, 12180–12186 (2013).
74. Kisch, H. Semiconductor photocatalysis for chemoselective radical coupling reactions. *Acc. Chem. Res.* **50**, 1002–1010 (2017).
75. Schneider, J. & Bahnemann, D. W. Undesired role of sacrificial reagents in photocatalysis. *J. Phys. Chem. Lett.* **4**, 3479–3483 (2013).
76. Shkrob, I. A. & Wan, J. K. S. Chemically induced dynamic electron polarization (CIDEP) spectroscopy of radicals generated in the photoreactions of polyols: the mechanisms of radical dehydration. *Res. Chem. Intermed.* **18**, 19–47 (1992).
77. Shkrob, I. A., Myran, C. S. J. & Gosztola, D. Efficient, rapid photooxidation of chemisorbed polyhydroxyl alcohols and carbohydrates by TiO_2 nanoparticles in an aqueous solution. *J. Phys. Chem. B* **108**, 12512–12517 (2004).
78. Copeland, J. R., Santillan, I. A., Schimming, S. M., Ewbank, J. L. & Sievers, C. Surface interactions of glycerol with acidic and basic metal oxides. *J. Phys. Chem. C* **117**, 21413–21425 (2013).
79. Jin, X. et al. Photocatalytic C–C bond cleavage in ethylene glycol on TiO_2: a molecular level picture and the effect of metal nanoparticles. *J. Catal.* **354**, 37–45 (2017).
80. Balducci, G. The adsorption of glucose at the surface of anatase: a computational study. *Chem. Phys. Lett.* **494**, 54–59 (2010).
81. Shkrob, I. A., Marin, T. W., Chemerisov, S. D. & Sevilla, M. D. Mechanistic aspects of photooxidation of polyhydroxylated molecules on metal oxides. *J. Phys. Chem. C* **115**, 4642–4648 (2011).
82. Sanwald, K. E., Berto, T. F., Eisenreich, W., Gutiérrez, O. Y. & Lercher, J. A. Catalytic routes and oxidation mechanisms in photoreforming of polyols. *J. Catal.* **344**, 806–816 (2016).
83. Wang, M., Liu, M., Lu, J. & Wang, F. Photo splitting of bio-polyols and sugars to methanol and syngas. *Nat. Commun.* **11**, 1083 (2020).
84. Zhang, Z., Wang, M., Zhou, H. & Wang, F. Surface sulfate ion on CdS catalyst enhances syngas generation from biopolyols. *J. Am. Chem. Soc.* **143**, 6533–6541 (2021).
This paper shows that bio-polyols can be transfromed to CO via sequential acyl-radical-mediated decarbonylation processes.

85. Pattanaik, B. P. & Misra, R. D. Effect of reaction pathway and operating parameters on the deoxygenation of vegetable oils to produce diesel range hydrocarbon fuels: a review. *Renew. Sustain. Energy Rev.* **73**, 545–557 (2017).
86. Gosselink, R. W. et al. Reaction pathways for the deoxygenation of vegetable oils and related model compounds. *ChemSusChem* **6**, 1576–1594 (2013).
87. Schwarz, J. & König, B. Decarboxylative reactions with and without light–a comparison. *Green Chem.* **20**, 323–361 (2018).
88. Manley, D. W. et al. Unconventional titania photocatalysis: direct deployment of carboxylic acids in alkylations and annulations. *J. Am. Chem. Soc.* **134**, 13580–13583 (2012).
89. Manley, D. W. & Walton, J. C. A clean and selective radical homocoupling employing carboxylic acids with titania photoredox catalysis. *Org. Lett.* **16**, 5394–5397 (2014).
90. Creusen, G., Holzhäuser, F. J., Artz, J., Palkovits, S. & Palkovits, R. Producing widespread monomers from biomass using economical carbon and ruthenium–titanium dioxide electrocatalysts. *ACS Sustain. Chem. Eng.* **6**, 17108–17113 (2018).
91. Huang, Z. et al. Enhanced photocatalytic alkane production from fatty acid decarboxylation via inhibition of radical oligomerization. *Nat. Catal.* **3**, 170–178 (2020).
This paper shows that alkane can be selectively produced from fatty acid decarboxylation via rapid radical hydrogenation over a hydrogen-rich catalyst surface.
92. Bahnemann, W., Muneer, M. & Haque, M. M. Titanium dioxide-mediated photocatalysed degradation of few selected organic pollutants in aqueous suspensions. *Catal. Today* **124**, 133–148 (2007).
93. Liao, Y. et al. The role of pretreatment in the catalytic valorization of cellulose. *Mol. Catal.* **487**, 110883 (2020).
94. Rinaldi, R. et al. Paving the way for lignin valorisation: recent advances in bioengineering, biorefining and catalysis. *Angew. Chem. Int. Ed.* **55**, 8164–8215 (2016).
95. Abu-Omar, M. M. et al. Guidelines for performing lignin-first biorefining. *Energy Environ. Sci.* **14**, 262–292 (2021).
96. Herron, J. A., Kim, J., Upadhye, A. A., Huber, G. W. & Maravelias, C. T. A general framework for the assessment of solar fuel technologies. *Energy Environ. Sci.* **8**, 126–157 (2015).
97. Davis, R. et al. Process design and economics for the conversion of lignocellulosic biomass to hydrocarbon fuels and coproducts: 2018 biochemical design case update (NREL, 2018).

Acknowledgements
The authors are grateful for financial support from the National Natural Science Foundation of China (22025206, 21991094, 21721004, 21690080), the Ministry of Science and Technology of the People's Republic of China (2018YFE0117300), the CAS-NSTDA Joint Research Project (GJHZ2075), Dalian Science and Technology Innovation Fund (2019J11CY009) and Dalian Institute of Chemical Physics (DICP I202009).

Author contributions
All authors contributed to writing, revising and discussing the content of the article.

Competing interests
The authors declare no competing interests.

Peer review information
Nature Reviews Chemistry thanks M. Kärkäs, P. Ruiz and the other, anonymous, reviewers for their contribution to the peer review of this work.